Computational Analysis of Non-Periodic Oscillations Using the Harmonic Balance Method

Payam Azadian

A Thesis
in the Department
of
Mechanical, Industrial and Aerospace Engineering

Presented in Partial Fulfillment of the Requirements
for the Degree of Master of Applied Science (Mechanical Engineering) at
Concordia University
Montreal, Quebec, Canada

December 2021

CONCORDIA UNIVERSITY

School of Graduate Studies

This is to certify that the thesis prepared

By: Payam Azadian

Entitled: Computational Analysis of Non-Periodic Oscillations Using the Harmonic Balance Method

and submitted in partial fulfillment of the requirements for the degree of

Master of Applied Science (Mechanical Engineering)

complies with the regulations of the University and meets the accepted standards with respect to originality and quality.

Signed by the final examining committee:

Dr. Muthukumaran Packirisamy — Chair

Dr. Muthukumaran Packirisamy — Examiner

Dr. Lan Lin — Examiner

Dr. Behrooz Yousefzadeh — Supervisor

Approved by

Dr. Sivakumar Narayanswamy, Graduate Program Director

December 16, 2021

Dr. Mourad Debbabi, Dean Faculty of Engineering and Computer Science

Abstract

Computational Analysis of Non-Periodic Oscillations Using the Harmonic Balance Method

Payam Azadian

This thesis investigates different approaches for applying the harmonic balance (HB) method to study steady-state non-periodic motion. The HB method is based on approximating the response of a nonlinear system using a truncated Fourier series. It is an established, powerful technique for analyzing and predicting the steady-state response of nonlinear systems.

The HB method is very popular in engineering because it reduces the cost of computations compared to direct numerical integration of the governing equations. This reduction is particularly important in nonlinear systems because the computational cost for these systems is typically much higher. Furthermore, the HB method can be used to approximate the steady-state quasi-periodic response of different types of systems. The quasi-periodic motion is characterized by two or more harmonic components with incommensurate frequencies. This type of motion can emerge in a mechanical system in response to two harmonic excitations with an irrational frequency ratio. The excitations can be external, internal (parametric), or a combination of the two. Since quasi-periodic motion is not periodic, it cannot be represented by a simple Fourier series. Therefore, specialized formulations are required for using the HB method for the analysis of quasi-periodic motion.

The objective of this work is to investigate different approaches for approximating the steady-state quasi-periodic response of mechanical systems using the HB method. In particular, we focus on two techniques: the multidimensional HB method and the trained HB method. The results are verified with direct numerical analysis and published literature results to show that the approximation error is acceptable. The problem formulations are discussed in the non-dimensional form to keep the results general. Various case studies are used to better demonstrate how the algorithms work.

Acknowledgment

I would like to thank my supervisor for guiding me through this process and my friends for their unwavering supports.

I wish to thank my loving and supportive wife, Avishan, and my wonderful son, Pendar, who provides unending inspiration.

Table of contents

List of Figures

Nomenclature

ACRONYM	DESCRIPTION
AFT	Alternating Frequency Time Domain
AHBM	Adjusted Harmonic Balance Method
ANF	Approximate Natural Frequency
DNI	Direct Numerical Integration
FPO	Forced Parametric Oscillation
HB	Harmonic Balance
IHB	Incremental Harmonic Balance
LSF	Lower Sideband Frequency
MHBM	Multidimensional Harmonic Balance Method
THBM	Trained Harmonic Balance Method
USF	Upper Sideband Frequency

SYMBOL	DESCRIPTION
$\otimes$	Kronecker tensor product
Δs	Curvilinear abscissa increment
C	Damping
f_{NL}	Generalize nonlinear force
$\mathrm{I_N}$	Identity matrix of size n
K	Stiffness
M	Mass
N	Number of samples from time domain
R	Residual function
x	Generalized displacement
α	Nonlinearity coefficient
Γ	Inverse Fourier transform matrix
ζ	Damping ratio
μ	Mass ratio
ω_n	Natural frequency

CHAPTER 1 Introduction, Literature Review and Objectives

1.1 Non-periodic motion and Harmonic Balance Method

Our daily life is under the effect of periodic dynamic systems same as the beating of our heart, the music we listen to, or the light we see. We usually start our daily routine based on the earth's axial rotation and arrange our yearly and future programs according to the planet traveling around the sun. Moreover, the seasons made by traveling around this planetary orbit are significant in the construction industry and agriculture. These repetitive variations are named periodic in general because their motion repeats in time. The period of this repetition can be more than 23,000 years for an ice age or less than 10^{-15}s for ultraviolet radiation. However, most of the natural oscillations do not have a fixed period. For instance, the polar motion of the earth does not have a specific period because it is affected by some complex phenomena with different frequencies. Three primary phenomena that affect it are Greenland-ice sheets melting during the summer, motion in the earth's core and mantle, and isostatic rebound from the glacial period [1]. The sum of these effects results in motion that cannot easily be categorized in periodic or non-periodic motion. Between these two types of motion, there is another kind of oscillation that is named almost periodic. Although the aperiodic motion is defined as a non-repeatable motion, the almost periodic motion can repeat in infinite time. Most of the natural dynamic systems are categorized in this new definition. For instance, one of the subsets of this type of oscillation is the quasi-periodic motion that defines climate oscillation, axial rotation of the earth, black hole X-ray binaries [2], and most of the dynamic systems that affect our daily life.

In more straightforward engineering examples, which are the focus of this thesis, the quasi-periodic motion may appear in a system that is excited by more than one periodic source. These sources can result in a nonperiodic motion if they oscillate with incommensurable frequencies. An example of this type of oscillation is a mechanism with two shafts that rotate at different speeds [3] or multi-spool aircraft engines [4]. From the mathematical point of view, if this oscillation is represented in the phase space by a torus, the curve never exactly comes back to itself. In other words, the quasi-periodic motion seems repeating, but it never repeats an exact plan.

If we consider the earth's rotation and its tilted axis again, we will find its effects on the whole live habitant living on it. The earth's tilted axis, plus its orbit around the sun, affects weather and daylight hours that create seasons. An important aspect of changing the temperature change during

the seasons is its maximum and minimum value, not its average or absolute value. The highest and the lowest temperature during the year specify which species can live in each region or the cost and difficulty of living for people. Moreover, it is essential to predict the next typhoon in Western Pacific to reduce its costs and damage. This multifrequency system's dynamic behavior will also seem more complex by adding a nonlinearity. In the real world, most natural systems have some kind of nonlinearity. The nonlinearity may change the behavior of these systems from periodic or almost periodic oscillation to chaotic. However, we can still categorize many of these phenomena in quasi-periodic motion by avoiding the chaotic situation.

Similar to the climate, the maximum and minimum amplitude of an oscillating mechanical system is an important design parameter in mechanical mechanisms. It is helpful to know the maximum amplitude of a jet engine's shaft to design its bearing. On the other hand, finding the frequency that results in minimum amplitude is important in the design of vibration isolators and absorbers. All these dynamic systems have two different states. The transient state appears in the initial state of vibration, then through time, is replaced by a stable steady state. Overall, analyzing the steady-state response is often more relevant than the transient response because design specifications are presented for the steady-state situation. There are two leading groups of methods for analyzing the steady-state behavior of a system. Firstly, the time-domain algorithms and secondly, the frequency-domain. The second group has an advantage in computational cost and the ability to predict the unstable response of a system. One of the famous members of this group is the HB method that is the object of this work.

Urabe [5], [6] put the cornerstone of the HB in 1964. However, the method did not become popular until the 1980s, since the contribution from Lau et al. [7]. They used HB as the incremental harmonic balance method to study a wide range of nonlinear differential equations. Therefore, today the HB is perhaps the most popular method for approximating the stationary nonlinear response of dynamic systems [8], [9], [10], [11]. In the first step, Urabe [5] presented the technique as the Galerkin method based a truncated Fourier series. His idea was quite simple but effective in solving many dynamic systems. A truncated Fourier series with a few terms can still achieves a reasonably accurate approximation of the response. By applying the series to the dynamic equation, a system of the equations yields that the Fourier coefficients are its unknowns. Urabe [6] used the Newton method for solving the algebraic equations numerically because the

equations become nonlinear in nonlinear problems. He also outlined the method developed later by Lau et al. [7] and is named by Cameron and Griffin [12] as alternating frequency time domain (AFT). This technique makes HB more computationally efficient in nonlinear problems.

The subsequent sections describe the HB method, AFT technique, and numerical continuation. The focus of these parts is on the analysis of periodic response. This makes it easier to explain the methodology, which forms the backbone of subsequent Chapters. The continuation method is used to predict the "bending" part of the frequency response curve, where the jump phenomenon occurs. The AFT method provides a means to avoid the complicated computations involved in classical Galerkin-based approach to the HB method. These two techniques (AFT and continuation) are used in other Chapters for different types of oscillators.

1.2 Classical Formulation

The general equation of motion which is used in present work is expressed as

$$M\ddot{x} + C\dot{x} + Kx + f_{NL}(x, \dot{x}, t) = g(t) \tag{1.1}$$

where *M*, *C,* and *K* stand for mass, damping, and stiffness, respectively. The x denotes the generalized displacement and f_{NL} represents the generalized nonlinear term that is a function of x, its derivation, and time. When the external excitation $g(t)$ is periodic, it can be represented as a Fourier series:

$$g(t) = \sum_{k=0}^{\infty} \tilde{A}_x \cos(k\omega t) + \tilde{B}_x \sin(k\omega t) \tag{1.2}$$

Or in the complex-exponential representation

$$g(t) = \sum_{k=-\infty}^{\infty} \tilde{C}_k e^{(ik\omega t)} \tag{1.3}$$

where the tilde sign $(\tilde{\ })$ is used to denote parameters in the frequency domain. The steady-state response of the system under this excitation can be represented as a complex Fourier series

$$x(t) = \sum_{k=-\infty}^{\infty} \tilde{a}_k e^{(ik\omega t)} \tag{1.4}$$

The idea of HB method is to use a truncated part of this series as an approximate response

$$x(t) \approx \sum_{k=-H}^{H} \tilde{a}_k e^{(ik\omega t)} \quad H \in \mathbb{N} \tag{1.5}$$

The substitution of this approximation in the governing equation (1.1) yields

$$(-\omega^2 M + iC\omega + K)\tilde{x} + F_{NL}(\tilde{x}) - \tilde{g} = \tilde{R}. \tag{1.6}$$

Eq. (1.6) is a system of nonlinear algebraic equations with $\tilde{x}$ as the unknown and $\tilde{R}$ as the residual function. The roots of this system of equations are often found using an optimization technique, whereby the local minima of $\tilde{R}$ correspond to the amplitudes of the steady-state response of the system. The Fourier coefficients on these local minimums present the amplitudes of the steady-state response of the system. The sine and cosine harmonic coefficients can be found by separating the real and imaginary parts of the equations. The HB method can also be applied using the sine and cosine functions instead of the complex notation used in Eq. (1.6). These two formulations are equivalent. The coefficients of the harmonic functions can be found from Eq. (1.6) by separating the real and imaginary parts of the equation. See Appendix A for more details.

Selecting the Harmonic Truncation Order, H in Eq. (1.5), depends on the physics of the system. Generally, the truncated Fourier series should describe phenomena associated with super-harmonic, sub-harmonic, or combination resonances. However, when the number of resonance frequencies is infinite, it is computationally advantageous to consider a subset of the system's order. Moreover, the frequency response of some systems includes only odd or even harmonics, which can halve the cost of processing.

1.2.1 The AFT technique

The AFT method is utilized to evaluate the nonlinear terms of the governing equation. This method returns the discrete Fourier transform of an estimated response to the time domain where the analytical expression of nonlinear terms is known. Then the updated estimates of the nonlinear terms are transformed back to the frequency domain. This process is repeated at each iteration to evaluate the approximation of nonlinear terms. The AFT method calculates only a finite sample in the time domain. Therefore, it is essential to use more than N=2H+1 samples to achieve the exact value of the Fourier coefficients in the frequency domain [8].

The inverse Fourier transform that is used in this work can be written as a linear operation:

$$x = \Gamma(\omega) \otimes I_N \, \tilde{x} \tag{1.7}$$

where $\otimes$ and I_N stand for the Kronecker tensor product and the identity matrix of size n, respectively, and the sparse operator $\Gamma(\omega)$ is:

$$\Gamma(\omega) = \begin{bmatrix} e^{-\frac{iH2\pi}{N}(0)} & \cdots & e^{\frac{iH2\pi}{N}(0)} \\ \vdots & \ddots & \vdots \\ e^{-\frac{iH2\pi}{N}(N-1)} & \cdots & e^{\frac{iH2\pi}{N}(N-1)} \end{bmatrix}. \tag{1.8}$$

An example for this matrix is represented in Figure 1.1 for fifteen harmonic terms (N=15). After calculating the nonlinearity in time domain, the result is transferred back to the frequency domain by:

$$x = \Gamma(\omega)^* \otimes I_N \, \tilde{x} \tag{1.9}$$

where $\Gamma(\omega)^*$ is:

$$\Gamma(\omega)^* = \frac{1}{N} \begin{bmatrix} e^{\frac{iH2\pi}{N}(0)} & \cdots & e^{-\frac{iH2\pi}{N}(0)} \\ \vdots & \ddots & \vdots \\ e^{\frac{iH2\pi}{N}(N-1)} & \cdots & e^{-\frac{iH2\pi}{N}(N-1)} \end{bmatrix} \tag{1.10}$$

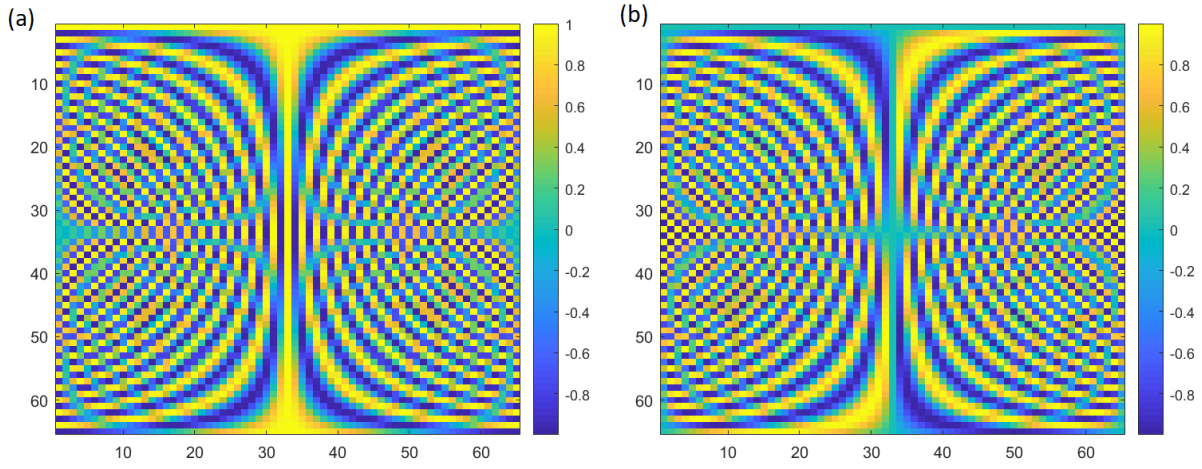

Figure 1.1: Illustration of the inverse Fourier transformation matrix for H=15, and N=65, (a) Real and (b) Image part.

This is an efficient way to compute the nonlinear terms and decrease the complexity of calculating the harmonic coefficients.

1.2.2 Numerical continuation

Optimization algorithms require an initial guess of the solution to converge quickly and avoid local minimums. By starting from zero (i.e., starting at initial rest from the equilibrium position), only the first local minimum of the system near zero can be captured. Often, this is not the global minimum of the equation that resulted from balancing the harmonics. Moreover, in contrast to linear systems, nonlinear systems may have more than one possible steady-state response for a fixed set of system parameters. In this case, the initial conditions determine which steady-state response is reached. The nonlinearity in stiffness moves the resonance frequency to the higher or lower frequencies due to hardening or softening in stiffness, respectively. This change in resonance frequency makes zones in the frequency response curve with more than one possible steady-state response. Those multi-response zones usually indicate at least two stable and one unstable response for each frequency. Computing the frequency response of the system always from equilibrium position would result in only the lower amplitude response and miss the other possible solutions. It is the same as the jump or hysteresis phenomenon in a dynamic system with hardening stiffness when the excitation frequency decreases gradually. In this case, the amplitude response of the system jumps to a higher value before resonance frequencies [13]. Therefore, peaks of the frequency response curve and unstable responses are not represented in response. The numerical continuation method can represent the system response as a continuous curve that includes the peak and unstable parts of the response [9].

A continuation technique consists of two parts: a predictor and a corrector. The secant, tangent, and Lagrange polynomials methods are three predictors that provide direction and distance. In the present work, the secant method is used because it is more efficient.

The secant method uses two previous points of the response curve. These points can be calculated by starting optimization from the equilibrium position when the response curve is smooth and far from resonance frequencies. Then by having these points, we can predict the other ones with the following equation.

$$\left(\tilde{x}^{(i+1,0)}, \omega^{(i+1,0)}\right) = \left(\tilde{x}^{(i)}, \omega^{(i)}\right) + \Delta s^{i+1}\left(\left(\tilde{x}^{(i)}, \omega^{(i)}\right) - \left(\tilde{x}^{(i-1)}, \omega^{(i-1)}\right)\right) \qquad (1.11)$$

where Δs^{i+1} is the curvilinear abscissa increment (see Figure 1.2(a)). For example, near the zero excitation frequency, the response curve is approximately parallel to the frequency axis and $\Delta s \cong$

$\Delta\omega$. In this situation, it is easy to predict the second point on the curve by assuming the $\Delta s = \Delta\omega$ and optimizing the equation to achieve the correct curvilinear distance.

The arc-length method (see Figure 1.2(b)) is used in this work as a corrector method to guide the optimization function to the correct point. This method adds the distance condition between the expected point and the previous converged point. The equation of this method is

$$||\tilde{x}^{(i+1,j+1)} - \tilde{x}^{(i)}||^2 + |\omega^{(i+1,j+1)} - \omega^{(i)}|^2 - \left(\Delta s^{(i+1)}\right)^2 = 0 \tag{1.12}$$

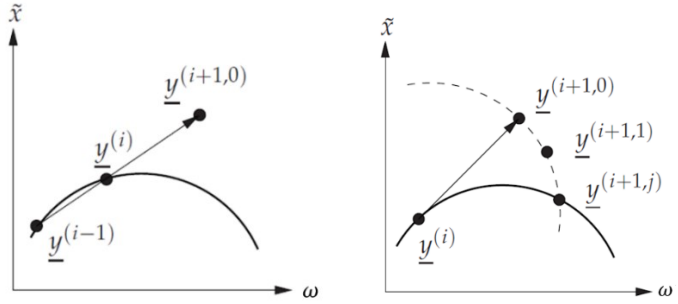

Figure 1.2: (a) Illustration of Secant predictor method and (b) Arc Length method.

The system of algebraic equations that result from the HB method is typically solved by a root-finding method, such as the Newton-Raphson procedure. In the present work, different types of optimization algorithms like trust-region [14], trust-region-dogleg [15], and Levenberg-Marquardt method [16]–[18] are used according to the complexity of the problem to reduce the computer time. These algorithms improve the Newton method by defining a region around the current best solution or searching the direction of the linear set of equations solution. Moreover, the trust-region-dogleg is the algorithm that is specially designed to solve nonlinear equations.

The curvilinear abscissa increment (Δs) must be adjusted during the continuation. This parameter affects the convergence of the optimization algorithm and, thereby, the time taken for computing the frequency response curve. For instance, if the optimization algorithm converges in less than three iterations, the step size can be doubled to predict the next point and avoid spending time in unnecessary steps in the smooth part of the response curve. On the other hand, if the number of iterations is more than a user-determined maximum number (for example, 10), the step size must be decreased to improve the accuracy in subsequent steps of computation (for example, divided by two). Finally, if the number of iterations is more than the maximum number determined by the user (for example, 15) or the optimization algorithm fails. The step size is

decreased, and the optimization process is repeated for the current point. This procedure decreases the step size in regions with high curvature and results in computation of a smooth curve. As a result of incorporating the above control over the step size to the code, the optimization algorithm converges at all steps.

1.3 Thesis layout

The rest of this thesis is organized in four Chapters and four appendices. Chapter 2 presents the formulation used to apply the HB method to an oscillator subject to two harmonic excitations with incommensurate frequencies. This requires a modification of the AFT method. The revised AFT method is used in conjunction with numerical continuation to compute the frequency response of a nonlinear system to bi-periodic excitation. After verifying the method with previous work and numerical results, we use it to compute the response of a system with two degrees of freedom degree of freedom.

In Chapter 3, we apply the HB method to compute the response of a parametrically excited system. The focus of this Chapter is on computing the periodic only. After verifying the method, it is applied to different types of oscillators with the periodic response. We study the effect of cubic and quadratic nonlinearity on the response of the system.

In Chapter 4, the HB method is applied to a parametrically excited system subject to an external harmonic force with a frequency that can be incommensurate with the frequency of parametric excitation. Therefore, the response of the system switches between periodic and quasi-periodic in this case. The method and the stability of the response are studied numerically. A problem arises by adding the nonlinear term to this system. The AFT method is useless here because of the non-harmonic nature of the system. Therefore, we present a solution without AFT and find the response curve. After verification, the method is used to test the reciprocity invariance in a system with two and more degrees of freedom.

Chapter 5 presents the conclusions and the suggested future works. The present study indicates that using the HB method to study the steady-state quasi-periodic response of a parametrically excited system is not straightforward. For this reason, there is a need to extend the present work.

CHAPTER 2 Systems Subject to Multiple Harmonic Excitations

2.1 Introduction

Multi-frequency nonlinear oscillation is a feature of many technical, industrial, and natural dynamical systems. This kind of behavior can be observed in many fields such as the biological system in biological sciences [19], the electromagnetic wave propagation in physical sciences [20], the micro/nano-electromechanical systems (MEMS/NEMS) in nano-technology and microsystems [21], the modulators and mixers in the communication circuits [22] or electric power system in the electrical engineering [23], and rotating machines and gears in the mechanical engineering filed [24], [25].

Many applications that involve rotating mechanisms (from hard drives in personal computers to aero-engines and large-scale power generators) exhibit multi-frequency vibration. For example, the multi-shaft aircraft engines are the issue of quasi-periodic motions that come from rotor imbalance exciting [26]. The ensuing vibrations can cause problems such as rotors touching seals, inter-shaft contact in multiple spool engines, rotor blades contacting the stator, and increased bearing clearance through wear or outright bearing failure [27]. For controlling the effect of these kinds of dynamic motions, understanding their steady-state response is necessary, which can help design lighter and more powerful engines.

The direct solution of the dynamic response of nonlinear system subject to multi-frequency excitation is often too costly because the numerical integration takes a long time for the transients to die out. Furthermore, the direct solution method cannot capture unstable frequency response branches.

Although several numerical methods are developed to study the steady-state response of nonlinear systems such as harmonic balance, shooting type, split frequency harmonic balance, and averaging, these methods were mainly developed to analyze periodic motion, and cannot be directly used for the analysis of quasi-periodic motion. For instance, the shooting method cannot be helpful when the system response is not periodic because the solution must be started from a periodic initial state and becomes laborious when the period of vibration is considerable compared to the singular frequency. Perturbation methods are restricted to weak nonlinearity, and therefore have a limited range of validity. The classical HB method has a very tedious formulation for nonlinear systems with high harmonic terms. It needs to know a priori in which harmonic terms ought to be included in the analysis to obtain a consistent solution. Therefore, new techniques

have been developed for approximating the result of these multidimensional excited nonlinear systems.

In 1981, Chua and Ushida [28] presented a generalization harmonic balance method for computing almost periodic response of multiple input frequencies electrical circuits. They found the steady-state response of the system by collocating trigonometrical equations and solved them as the multidimensional harmonic balance method (MHBM). In 1983, Lau and Cheung [7] developed the incremental harmonic balance formulation (IHB) that based on linearizing the equations in each step. In 1996, Kim and Noah [27] improved this approach by using FFT for transferring equations between the time and frequency domains. In 2004, Pusenjak and Oblak [29] used arc length continuation for finding the bifurcation diagrams of MHBM.

In 2012, Guskov and Thouverez [30] presented the adjusted harmonic balance method (AHBM) to overcome the difficulty of complex matrix operations that are needed to find the coefficients of the Fourier series in MHBM. They used a one-dimensional Fourier series that was expressed by the greatest common divisor of two excitation frequencies. But this approach requires a higher number of harmonic terms to achieve the same accuracy as MHBM.

In 2019, Prabith and Praveen Krishna [31] extended a Time Variational Method (TVM) that had been presented as an alternative method to the AFT by Rook [32] to multiple-frequency excitation. Compared to MHBM-AFT, this new technique was improved by taking advantage of the correlated nature of nonlinear force and displacement of Fourier coefficients. The main advantage of TVM to MHBM-AFT is that it does not require transformation between the frequency and time domains. In addition, TVM automatically includes the required harmonics in this formulation and avoids the trouble of selecting a suitable number of harmonics. The main drawback of the TVM appears when the system has a strong nonlinearity. In this situation, a large number of sampling points are required in the time domain to capture the response accurately.

Recently, Liao, Zhao, and Fang [33] determined the stability of quasi-periodic motion using the MHBM-AFT they improve the accuracy of computing the bifurcation diagrams by using the nonlinearly constrained optimization method instead of the Newton-Raphson method. By this change the methodology become more suitable for industrial.

In this Chapter, a code is developed in MATLAB to find the steady-state multi-harmonic response of a nonlinear system subject to multiple external harmonic forces. The MHBM-AFT was coupled with the Arc-Length method as the predictor-corrector continuation framework for

computing the bifurcation. The Newton-Raphson method is replaced by the Levenberg-Marquardt nonlinear optimization method to improve the convergence rate. The exponential form of the FFT and Jacobian matrix presented by K. Malta and G. Johann [8] is used in this work. The final code is a mix of the best results of previous works on this issue.

2.2 The Multidimensional Harmonic Balance Method

The steady-state response of a system subject to multiple external harmonic excitations can be represented as

$$x(t) = \sum_{k\in\mathbb{Z}^m}^{\infty} \tilde{a}_k e^{(k\omega t)} \qquad \omega = [\omega_1, \dots, \omega_m]^T \in \mathbb{R}^m \tag{2.1}$$

where **m** denotes the number of time/frequency dimensions, and the ω stands for the frequency basis. The $k = [k_1, \dots, k_m]$ represents the vectoral harmonic indexes. For example, the harmonic terms frequency distribution for 13 harmonics and two excitations are shown in Figure 2.1.

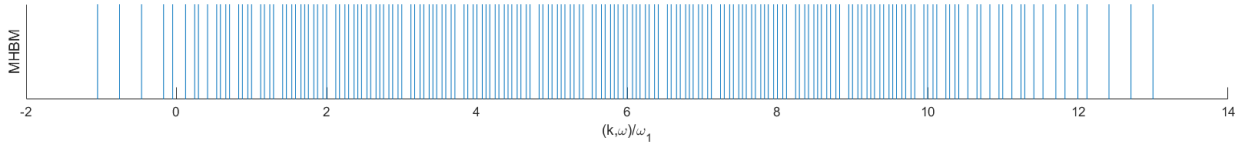

Figure 2.1: The distribution of the frequency terms retained in the multi-harmonic expansion of the response with m=2 and H=13.

As some of the harmonic indices are complex conjugate, truncating the harmonic terms is carried out in several ways. Three examples of the truncated set for m=2 and N=5 is shown in Figure 2.2. The full set of indices for a given N corresponds to the following condition:

$$\sum_{i=1}^{m} |k_i| \leq N. \tag{2.2}$$

Including the full set of indices is not necessary for capturing the response accurately. Following Legrand [34] and Liao et al. [33], we use the half indices set to validate our formulation (see Figure 2.2). Subsequently, we use the set proposed by Chua and Kim to significantly decrease the computational cost while retaining the results' accuracy.

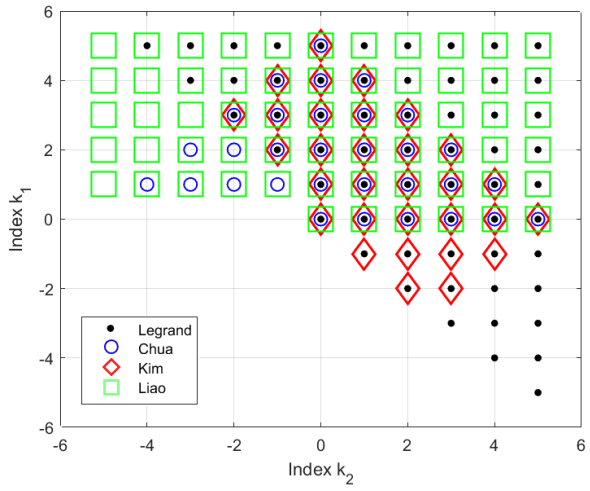

Figure 2.2: Harmonic indices sets.

2.3 AFT technique for multi-frequency problem

A multi-dimensional Fourier transfer matrix is required for solving the equations resulting from the MHBM. As the complex form of the Fourier series is used for the HB method, the complex multi-dimensional Fourier transfer matrix is used for the AFT method in MHBM. The two-dimensional complex Fourier transfer matrix and its inverse are detailed as follows (According to Ref. [33]):

$$\Theta = \begin{pmatrix} e^{2\pi i(k^{-N_k},\tau^1)} & \dots & e^{2\pi i(k^{-1},\tau^1)} & 1 & e^{2\pi i(k^1,\tau^1)} & \dots & e^{2\pi i(k^{N_k},\tau^1)} \\ e^{2\pi i(k^{-N_k},\tau^2)} & \dots & e^{2\pi i(k^{-1},\tau^2)} & 1 & e^{2\pi i(k^1,\tau^2)} & \dots & e^{2\pi i(k^{N_k},\tau^2)} \\ \vdots & \ddots & \vdots & \vdots & \vdots & \ddots & \vdots \\ e^{2\pi i(k^{-N_k},\tau^{N_t})} & \dots & e^{2\pi i(k^{-1},\tau^{N_t})} & 1 & e^{2\pi i(k^1,\tau^{N_t})} & \dots & e^{2\pi i(k^{N_k},\tau^{N_t})} \end{pmatrix} \tag{2.3}$$

$$\Theta^{-1} = \frac{1}{N_\tau}\begin{pmatrix} e^{2\pi i(k^{-N_k},\tau^1)} & e^{2\pi i(k^{-N_k},\tau^2)} & \dots & e^{2\pi i(k^{-N_k},\tau^{N_t})} \\ \vdots & \vdots & \ddots & \vdots \\ e^{2\pi i(k^{-1},\tau^1)} & e^{2\pi i(k^{-1},\tau^2)} & \dots & e^{2\pi i(k^{-1},\tau^{N_t})} \\ 1 & 1 & \cdots & 1 \\ e^{2\pi i(k^1,\tau^1)} & e^{2\pi i(k^1,\tau^2)} & \dots & e^{2\pi i(k^1,\tau^{N_t})} \\ \vdots & \vdots & \ddots & \vdots \\ e^{2\pi i(k^{N_k},\tau^1)} & e^{2\pi i(k^{N_k},\tau^2)} & \dots & e^{2\pi i(k^{N_k},\tau^{N_t})} \end{pmatrix} \tag{2.4}$$

According to Guskov and Thouverez[30], 32 sample points are enough to model the MHBM for bi-harmonic excitations. The numerical example of Eq. 2.3 with the 32 sample points and five harmonic terms are depicted in Figure 2.3. This example is the same as what we use for the AFT technique in this work.

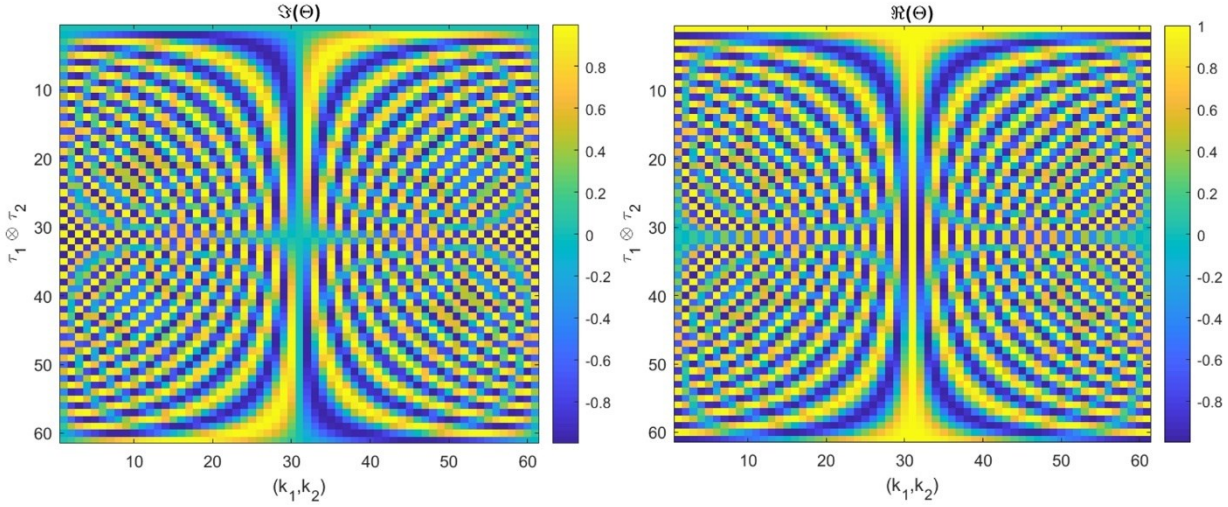

Figure 2.3: The imaginary and real parts of two-dimensional complex Fourier matrix.

2.4 Validation: The Duffing oscillator

The Duffing oscillator, named after Georg Duffing [35][36], is a nonlinear system that is used to explain the methodology. The Duffing equation is characterized by a nonlinear stiffness term, in which the nonlinear force is proportional to the third power of the deformation. The Duffing oscillator, subject to two external harmonic forces can be written as:

$$\ddot{x} + 2\zeta\dot{x} + x + \alpha x^3 = g_1 \sin(\omega_1 t) + g_2 \sin(\omega_2 t) \tag{2.5}$$

where the ζ and α stand for the damping ratio and nonlinearity coefficient. In this section, we have chosen the following values for the parameters of Eq. (2.5)

$$\zeta = 0.1, \qquad \alpha = 0.2, \qquad g_1 = g_2 = 5 \tag{2.6}$$

these values are chosen to be the same as those in Ref. [30] so that we can validate our results. The external forces in Eq. (2.5) can be represented in the complex form as:

$$\frac{g_1}{2i}\left(e^{i\omega_1 t} - e^{-i\omega_1 t}\right) + \frac{g_2}{2i}\left(e^{i\omega_2 t} - e^{-i\omega_2 t}\right) \tag{2.7}$$

The relationship between the two excitation frequencies is chosen to be an irrational number to ensure the response is quasi-periodic:

$$\frac{\omega_1}{\omega_2} = \sqrt{2} \approx 1.4142 \tag{2.8}$$

The frequency response of the system when it is subject to each of the two external forces individually is shown in Figure 2.4. This result shows the periodic response for both excitations under the effect of nonlinearity. The principal resonance peak and super harmonics are represented for both external frequencies. In this case, the first 15 harmonic terms are used to approximate the response of the Duffing oscillator; therefore, the seven super harmonics appear in the result (see Figure 2.4 insets). Figure 2.5 shows the quasi-periodic response of Eq. (2.5) using different numbers of harmonic terms that are indexed according to the Chua set. As expected, the combination resonances between two principal resonance and super harmonics that appear at lower frequencies can be captured if the appropriate harmonics are included in the truncated Fourier series in Eq. (2.1) (see Figure 2.5 inset). Both of these results have good agreement with Guskov and Thouverez's [30] work.

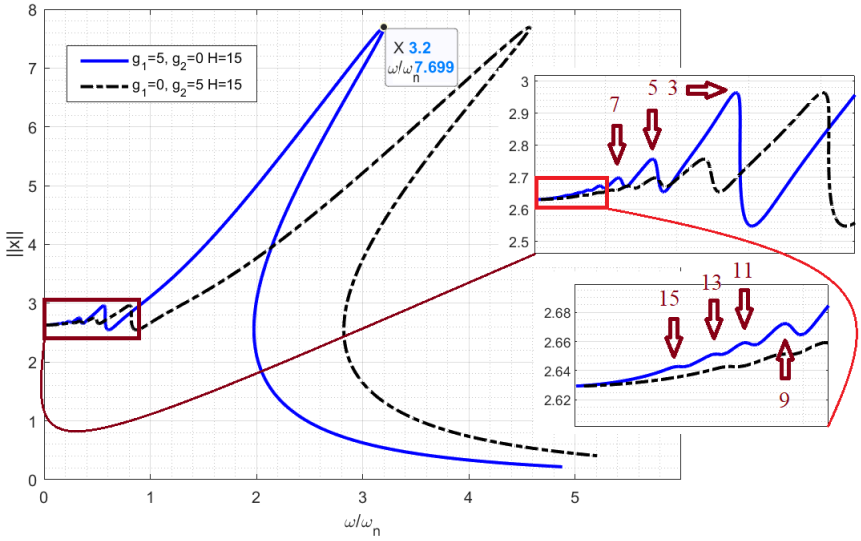

Figure 2.4: Response of Duffing oscillator to each harmonic component of the excitation separately.

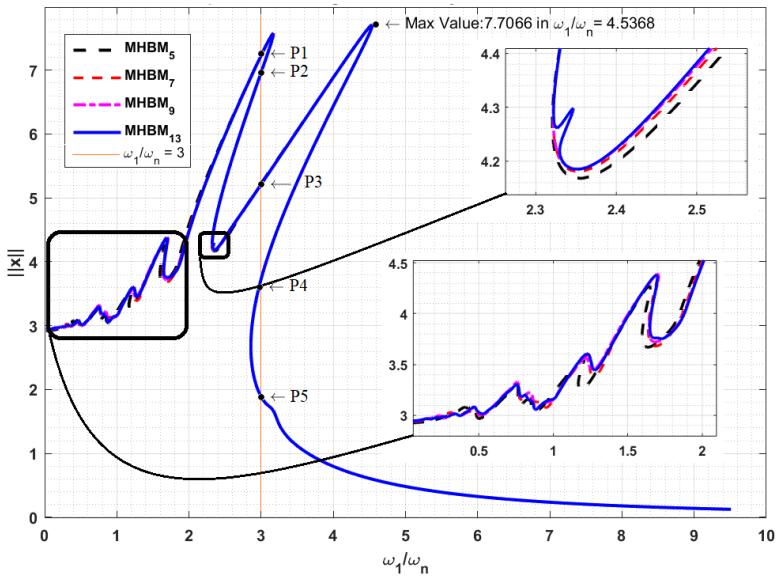

Figure 2.5: Response curves with different number of harmonic terms.

In the case of quasi-periodic motion, only a quarter of the harmonic indexes is used (Chua set same as Figure 2.2(a)), and as illustrated in Figure 2.6(a) for a peak in $\omega_1/\omega_n = 0.84$, the other indexes are omitted. However, the answer is only two percent less than a solution with all harmonic indexes (the same as the index in Figure 2.2(b)) that is shown in Figure 2.6(b). At the peak of the frequency response curve, with a lower effect of super-harmonics, the Chua set would become more accurate (see Figure 2.7) with less than 0.002 percentage error in comparison to the solution that used all the harmonic indexes.

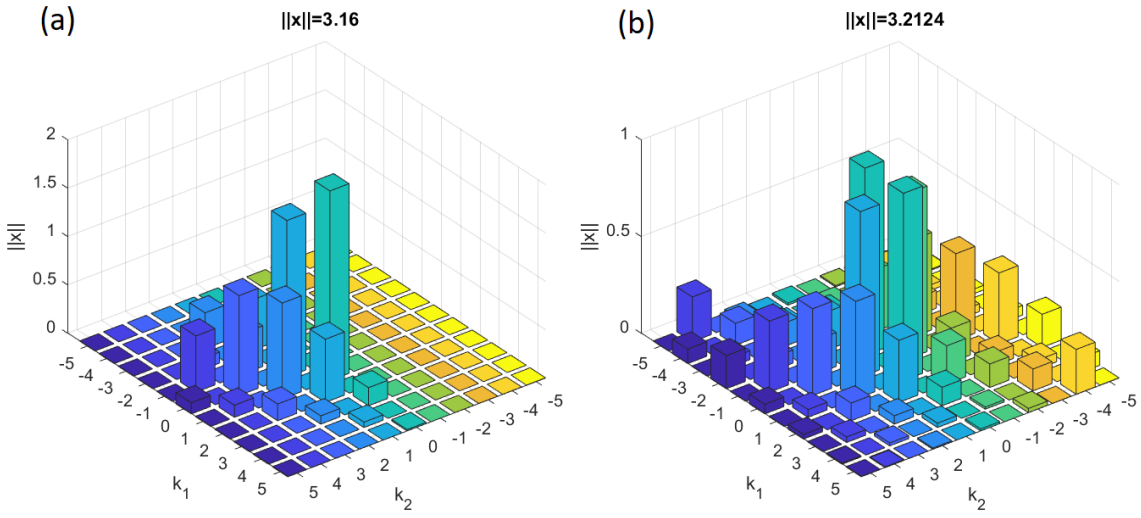

Figure 2.6: Response of the Duffing oscillator, (a) with Chua set and (b) with all subharmonic terms. The result of (a) shows only a 1.6% error in comparing with (b) ($\omega_1/\omega_n = 0.8375\ for\ a\ and\ 0.84106\ for\ b$).

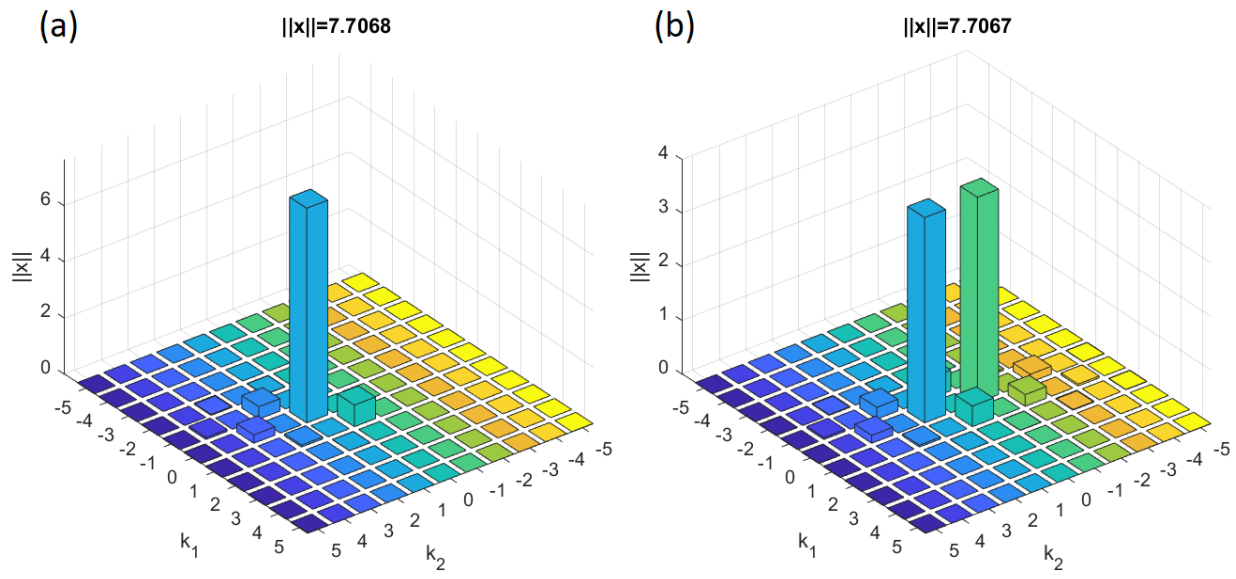

Figure 2.7: Response of the Duffing oscillator, (a) with Chua set and (b) with all harmonic terms The result of (a) shows only a 0.0013% error in comparing with (b) ($\omega_1/\omega_n = 4.5321\ for\ a\ and\ 4.5369\ for\ b$).

Five points with the same frequencies are selected on the frequency response curve to verify the results (see Figure 2.5 P1 to P5). Different sets of initial values need to be used when integrating Eq. (2.5) in time (DNI) to reach different steady-state amplitudes. Therefore, the result of the MHBM is used as an initial guess for the DIN method. This initial condition assists the DNI solution to reach the steady-state predicted by the HB method, the same as the result of P1 and P5 in Figure 2.8. In unstable points, the DNI solution that started from the MHBM initial guess gradually converges to the lower stable amplitude. That is the situation is showed in Figure 2.8 for the P2:P4. This stable response equals the last selected point's response, located in the lowest potential (P5), that shows as a result of integration in time from the equilibrium position. Finally, all solutions show the same time and frequency domains responses on the last stable point with the lowest amplitude. Moreover, the result of these tree solutions is compared in the frequency domain by Fourier transfer. This comparison shows the matching of the MHBM and the DNI with initial guess in stable points (see Figure 2.8 FFT of P1 and P5).

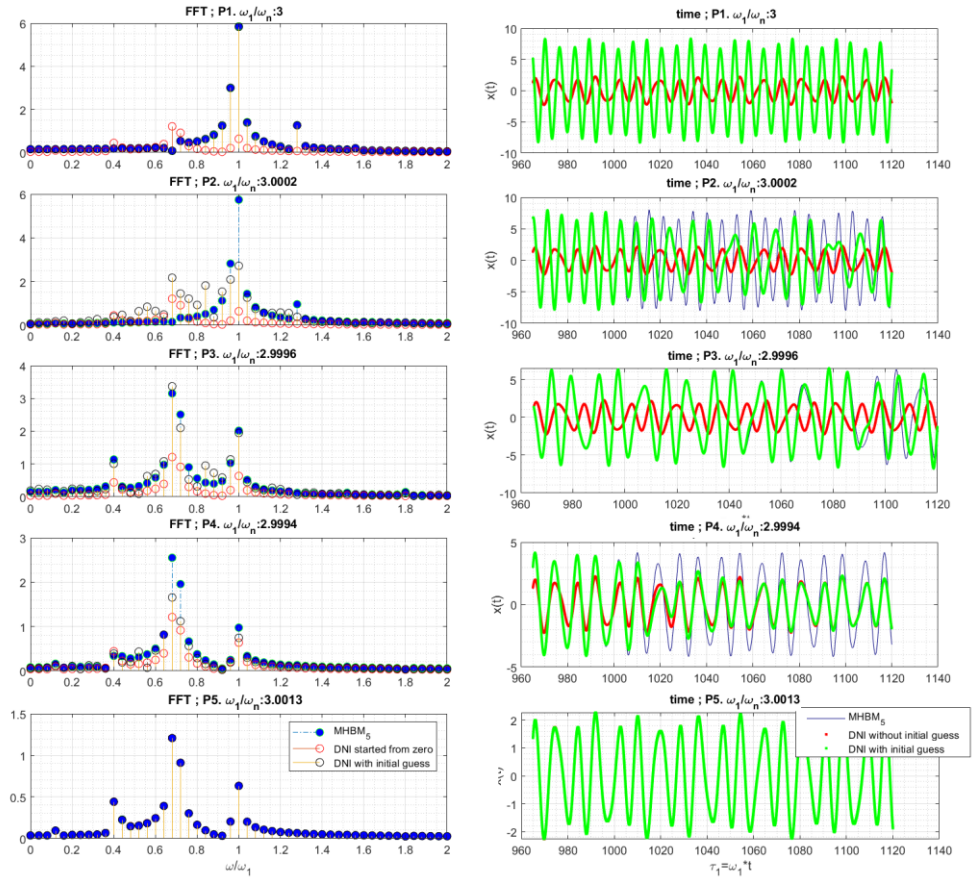

Figure 2.8: Time marching test for several points of the response curve (Fig.2.5) and respective FFT.

2.5 Coupled Duffing oscillators

The formulation developed in this Chapter is not restricted to systems with a single degree of freedom. To show this, we analyze the response of a system with two degrees of freedom. The system, shown in Figure 2.9, consists of a Duffing oscillator with an additional mass (m_2) attached to it through a linear spring (k_2) and a linear viscous damper (c). The external force acts on the first mass only and has two harmonic components with incommensurate frequencies. The equations of motion for this system are:

$$\ddot{x}_1 + 4\zeta\dot{x}_1 - 2\zeta\dot{x}_2 + (1+k_c)x_1 + \alpha x_1^3 - k_c x_2 = g_1 sin(\omega_1 t) + g_2 sin(\omega_2 t) \qquad (2.9)$$

$$\mu\ddot{x}_2 + 2\zeta\dot{x}_2 + k_c x_2 - k_c x_1 = 0 \qquad (2.10)$$

The following values are chosen for the system parameters:

$$k_c = 1, \alpha = 0.2, \mu = 1, \frac{\omega_1}{\omega_2} = \sqrt{2}, \zeta = 0.1, g_1 = g_2 = 5, \qquad (2.11)$$

The result of applying MHBM to the governing equation is verified by DNI, which shows a good agreement for 5 harmonic terms (see Figure 2.10). Comparing the peak of Figure 2.5 and the results in Figure 2.10(a) shows the second mass causes a reduction in the amplitude of the first one, like an absorber. The second mass experiences two resonances due to external forces and quasi-periodic motion without the effect of nonlinearity. An example of the second mass quasi-periodic motion is illustrated in Figure 2.11.

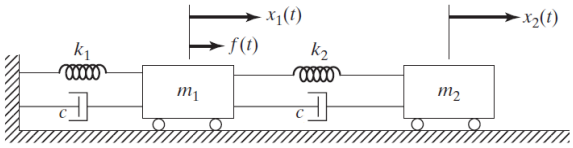

Figure 2.9: A two-degree-of-freedom system with external excitations.

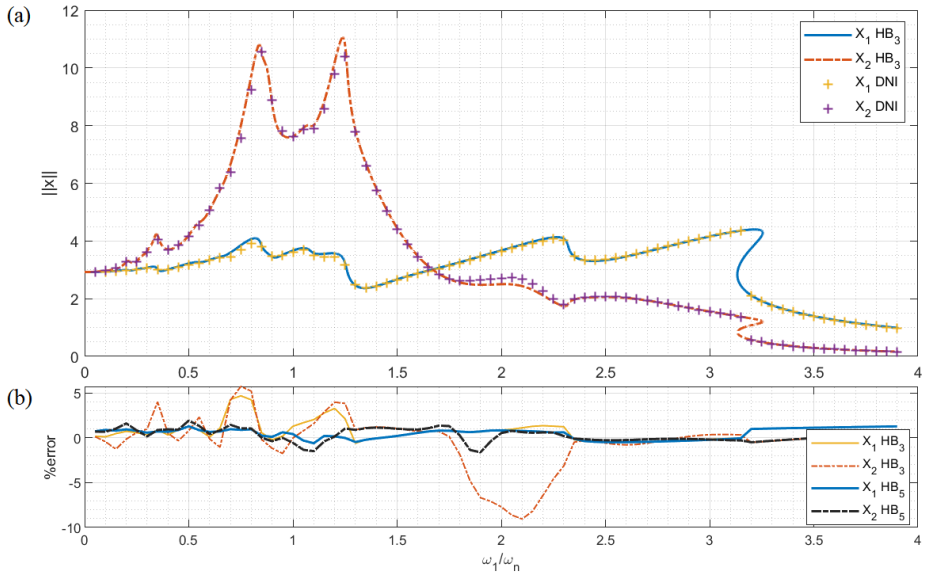

Figure 2.10: The 2D duffing oscillator. (a) The steady-state frequency responses of MHBM and DNI. (b) The error of comparing the result of MHBM with DNI.

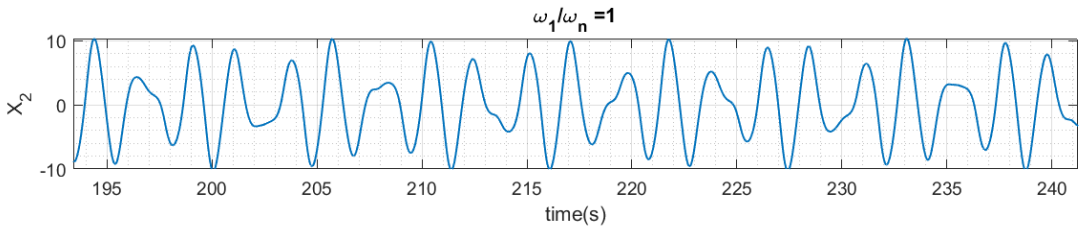

Figure 2.11: An example of quasi-periodic motion of second mass.

In this example, the average time cost of MHBM with Chua set is about a third of DNI or the result of solution with Liao set (see Figure 2.12).

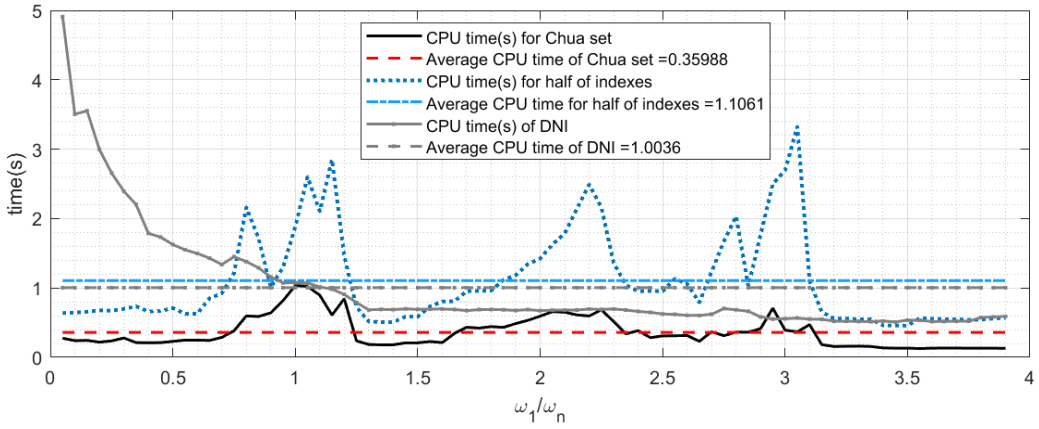

Figure 2.12: The CPU timing of different solutions (CPU: Intel(R) Core(TM) i7-1065G7 @ 1.30GHz 1.50 GHz).

2.6 Summary

In this Chapter, the MHBM was explained and used to capture the frequency response of the Duffing equation subject to incommensurate external excitations. We explained efforts to characterize and analyze the multifrequency dynamic system by starting from some background. We mixed all the previous beneficial techniques to achieve a better way of using the MHBM. After explaining the reasons for the new technique, we used in this work, the AFT method was modified by identifying which frequencies are expected to appear in the response. In part four, the frequency response of Duffing equation with incommensurate relation between external excitation frequencies was found and verified by previous works. Subsequently, the effect of selecting a different number of harmonic components on the result was discussed. As a result, except for the details of super-harmonics and combination resonance, it is possible to achieve an acceptable approximation for peaks with only three harmonic terms. For more clarifying, sample points of frequency response curve with the same frequency were selected to verify by the DNI method, which showed the same response in the stable points. Finally, we used the MHBM to analyze the frequency response of coupled Duffing oscillator as a case study at the end of this Chapter.

In conclusion, this Chapter showed the potential of the method based on the HB technique to predict the quasi-periodic motion in multi excitation systems. Although the MHBM takes significant computation time for the higher number of harmonic terms, it remains helpful in showing the steady-state frequency response in unstable situations.

CHAPTER 3 Systems Subject to Parametric and External Excitation: Periodic Oscillations

3.1 Introduction

Parametric oscillations appear when one of the parameters of a mechanical system (such as the effective stiffness) vary periodically with time. A familiar example of this type of vibration is a child pumping a swing. As the child is trying to get the swing going, the moment of inertia of the swing (i.e., the restoring force) is varied by the child's movements. As a result of this form of excitation, the swing starts moving, and its amplitude increases with time [37]. The dynamic behavior of a parametrically excited system becomes more complicated if an external harmonic force excites the system. This type of forced parametric vibration appears in many structures. It can be a destructive phenomenon in large size structures such as a twin-tail aircraft [38] or wind turbine blade [39]. In the small micro-electromechanical cantilever beams, this type of oscillation can be utilized in operation of electrical amplifier. For instance, J. Shaw and S. Shaw [40] represented the advantages of this oscillator with the nonlinear behavior to achieve a low-noise parametric amplifiers based on micro- and nano-systems.

Whether the excitation forces are artificial or made by natural phenomena, their effects on the system must be understood and controlled. Also, utilizing the effects of nonlinearities purposefully needs knowledge about the steady-state response of the system. Consequently, predicting the system's behavior is essential at the design stage to avoid failure or adjust the amplifier response. As the direct solution of the related equation is often too costly, several approximate methods have been studied to analyze the steady-state response of the parametrically excited systems. Perturbation, averaging, and Multiple time scales [40], [41] are methods that we typically use for predicting the behavior of this type of vibration system. Still, they are limited to a specific range of system parameters. Recently, Neumeyer et al. [42] used the varying amplitudes method to investigate the effect of cubic and quadratic nonlinearity on a parametric amplifier with perfect tuning. That method is so close to harmonic balance (HB) used in the present work.

Characterizing the frequency response of the force parametric oscillator with and without nonlinearity is the aim of this Chapter. The classical HB method is selected for this part since it is valid over a wide parameter range and is expected to capture the system's nonlinear behavior. Assuming the parametric frequency as an integer multiple of the external force frequency makes

periodic response for this problem. Without this relation, the response is quasi-periodic, which is the subject of the next Chapter. This Chapter consists of two main parts that cover solutions of linear and nonlinear forced parametric oscillations (FPO's) with periodic responses. In the linear solution part, the effect of an external harmonic force on the Mathieu equation is studied in stable and unstable frequency response zones and some examples are demonstrated in this part. The capability of the HB method to capture the different types of nonlinearities is the issue that is investigated in the next part.

3.2 Mathieu Oscillator Subject to External Excitation

This section applies the HB method to the FPO in different conditions with periodic responses, and results are verified by the DNI method and previous works. Also, the unique abilities of the HB method are discussed.

The equation of the motion of a system with parametric and external excitation is described by the following equation:

$$\ddot{x} + 2\zeta\dot{x} + k(t)x = Fcos(\omega_f t + \phi) \tag{3.1}$$

where ζ is the damping ratio, F and ω_f are direct excitation amplitude and frequency, t is time and

$$k(t) = k_0 + k_m \cos(\omega_m t), \tag{3.2}$$

where the k_0 is the stiffness, and the k_m is the parametric excitation amplitude. In this Chapter, ω_m is selected equal to two times $2\omega_f$ and k_0 equal to one. The fixed, integer ratio between the frequencies of parametric and direct excitations allows the steady-state response of the system to be periodic. We relax this condition in Chapter 4.

According to the frequency spectrum of the DNI method, the coefficients of even harmonic terms will be zero, and only the odd harmonic terms affect response. In addition, the relationship between external and parametric excitations result to harmonic response. Therefore, the steady-state response to such a system can be represented as:

$$x(t) \approx \sum_{k=1}^{H} \tilde{a}_k \cos(\omega_f t) + \tilde{b}_k \sin(\omega_f t) \;\; H \in (2\mathbb{N} + 1). \tag{3.3}$$

Substituting Eq. (3.3) in Eq. (3.1) and equating the coefficients of the terms with the same frequency results in a system of algebraic equations for the unknown amplitudes. The frequency response function is then obtained by solving the resulting system of equations.

The results obtained from using the HB method are validated by comparing them to the steady-state response of the system obtained by direct numerical integration of the governing equations. This validation is divided into two parts because the system has different behaviors above and below the system instability threshold. Suprathreshold pumping causes instability near the primary resonance frequency of the system that is not achievable by direct numerical integration. According to Rhoads and Shaw [40] the value of this threshold in a perfect tuning oscillator is equal to 4ζ for the amplitude of parametric excitation (k_m). When the system is below the parametric instability threshold, the response of the system is stable in all frequencies and comparable with the DNI method. Figure 3.1(a) presents the result of this comparison for $\phi = -\frac{\pi}{4}$. The HB method sometimes overestimates and sometimes underestimates the response frequency with a small error that is shown in Figure 3.1(b). As a second part of verifying, the system's frequency response above the parametric instability threshold is compared to the DNI (see Figure 3.2). All the system's coefficients and parameters are selected equal to Neumeyer et al.[42] to verify this internal curve. Therefore, the result presented in Figure 3.2Figure 3.2 is the same as that work. This response has some unstable points which can not be compared by the DNI results, but there is an excellent agreement in the other frequencies. These unstable responses arise below the systems instability threshold as an internal loop. For more clarifying, this internal curve is assumed as a loop because of the shape of the DNI response curve during the time in those unstable frequencies. During the time, the DNI curve grows with a similar shape as Figure 3.1(a) and never touches another branch called the internal loop.

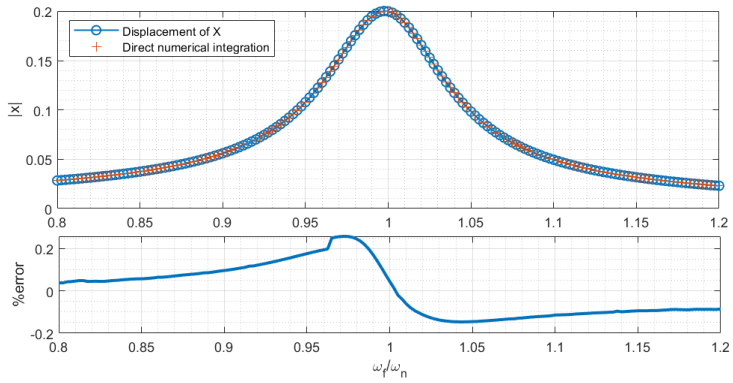

Figure 3.1: (a) Verifying the HB method frequency response by DNI, (b) error percentage of this comparing (k_0=1, k_m=0.1, ζ =0.05, F=0.01, H=7).

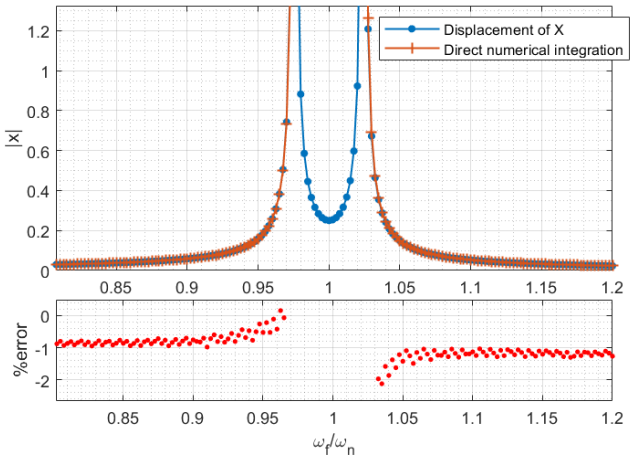

Figure 3.2: The frequency response of the system above the parametric instability threshold (k_0=1, k_m=0.1, ζ =0.005, F=0.01, H=7).

Figure 3.3shows a steady-state response of the system at $\omega_f = 0.5$. The periodicity of the response is due to the fixed ratio between the parametric and external frequencies. To verify the periodicity of the response, the Fourier transform of the displacement response is calculated and shown in Figure 3.4. We observe that the frequency spectrum of the steady-state response contains only the even harmonic of the external excitation.

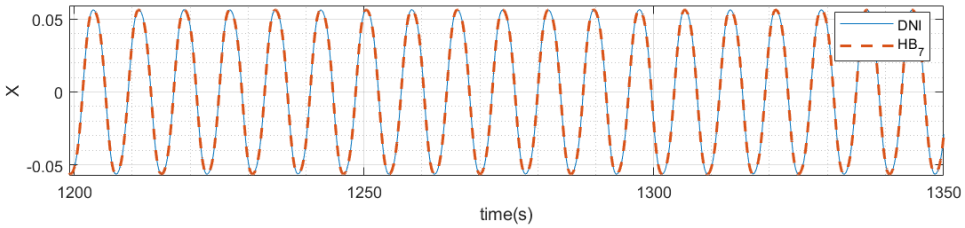

Figure 3.3: The time response for $\omega_m = 2\omega_f$ (k_0=1, k_m=0.5, ζ =0.005, F=0.01).

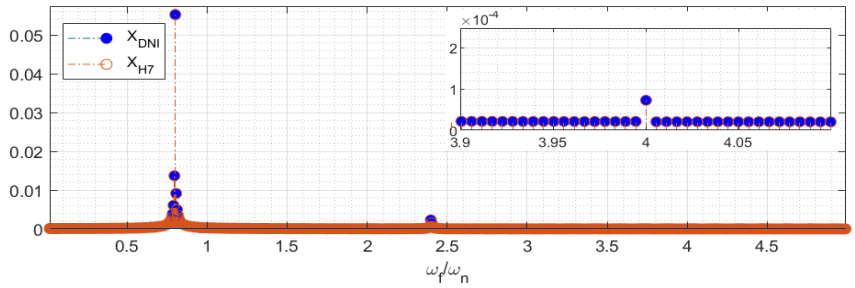

Figure 3.4: The frequency spectrum for $\omega_m = 2\omega_f$ in $\omega_f/\omega_n = 0.8$ (k_0=1, k_m=0.5, ζ =0.005, F=0.01).

Figure 3.5 shows the frequency response curves at different values of the damping coefficient close to the critical damping. The internal loop appears precisely in critical damping and grows by decreasing the damping coefficient. Moreover, this solution method is valid over a large parameter range, as shown in Figure 3.6. Both of these figures truncate to focus on the point system transfer from stable oscillator to the system with unstable behavior in resonance zone.

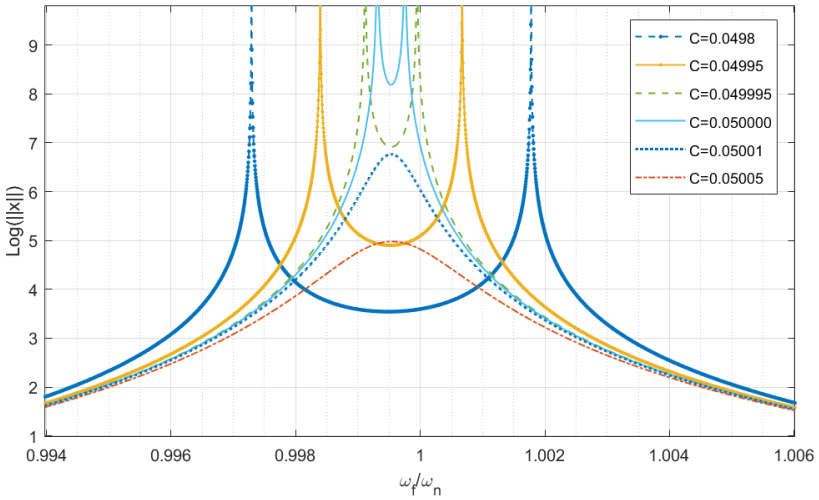

Figure 3.5: The frequency response around the critical damping point (k_0=1, k_m=0.1, F=0.01, H=5).

As long as the response remains harmonic, the HB can be used to obtain the steady-state response of the system. For example, Figure 3.7 shows the frequency response of the system for $\omega_m = 3\omega_f$, for different values of damping.

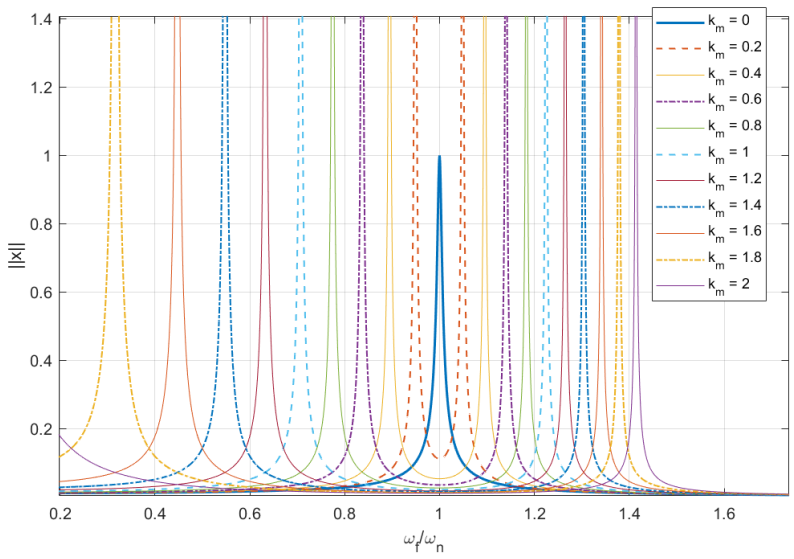

Figure 3.6: An amplitude response curve for different values of k_m (k_0=1, ζ =0.005, F=0.01, HB=5).

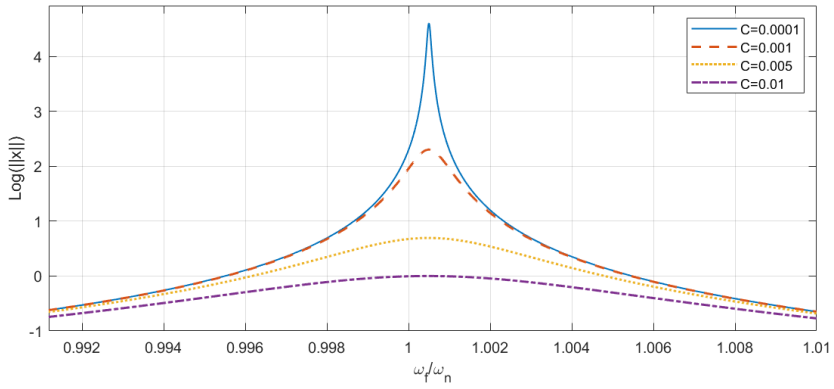

Figure 3.7: The frequency response of the system for $\omega_m = 3\omega_f$ (k_0=1, k_m=0.1, F=0.01, H=5).

Figure 3.8(a) shows the frequency response of the system for value of ω_m smaller than ω_f. Therefore, the response can be approximated as:

$$x(t) \approx \sum_{k=1}^{H} \tilde{a}_k \cos(\omega_m t) + \tilde{b}_k \sin(\omega_m t) \;\; H \in \mathbb{N}. \tag{3.4}$$

Figure 3.8(b) shows the error in the frequency response curve with respect to the results obtained from direct numerical integration of Eq. (3.1). The peak of the error's curve on $\frac{\omega_{f1}}{\omega_n} = 0.15$ is caused by super-harmonics at $6\omega_m$. The error can be reduced by including more harmonic terms (higher value of H) in Eq. (3.4). Figure 3.8(a) shows some super-harmonic peaks at low frequencies and one sub-harmonic, which do not exist in previous examples. According to the

appendix B and the frequency spectrum of DNI method, frequencies appear in the response of parametric oscillator are expected to be sub harmonic of series that can be shown as:

$$\omega = \omega_f - H\omega_m \; H \in \mathbb{N} \tag{3.5}$$

In this case, only this unique sub-harmonic exists, because (according to Eq.3.5) the second one is always equal to zero frequency and out of resonance. The third one behaves like the first one, and other lower harmonics are equal to primary resonance and super-harmonics, respectively. Therefore, it is expected that the oscillator with $3\omega_m = \omega_f$ has peaked in two sub-harmonics. When the parametric and external excitations are not harmonic (the issue of Chapter 4), the response frequency spectrum cannot be explained by sub and super-harmonic because of their non-harmonic nature. In this case, we suggest using Lower Sideband Frequency (LSF) Instead of sub-harmonic and upper sideband frequencies (USF) Instead of super-harmonic.

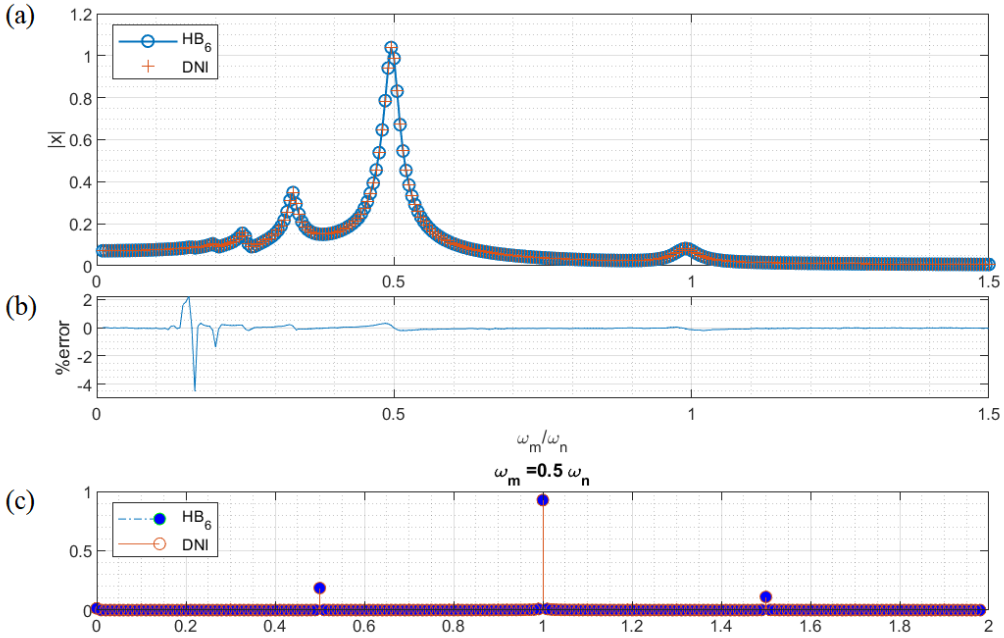

Figure 3.8: (a)The response of HB method verifying by DNI in frequency domains (b) for oscillator with the parametric frequency equal to half of the external excitation frequency ($\omega_m = 0.5\omega_f$, k_0=1, k_m=0.3, ζ =0.025, F=0.01, H=5).

The HB method can be used to analyze the response of a system with more than one external or parametric harmonic force. For example, assume the following governing equation

$$\ddot{x} + 2\zeta\dot{x} + k_0 + k_m \cos(\omega_m t)\, x = F_1 cos\left(\omega_{f1} t\right) + F_2 cos(\omega_{f2} t) \tag{3.6}$$

where $\omega_{f2} = 2\omega_m = 4\omega_{f1}$. Therefore, the response can be approximated as:

$$x(t) \approx \sum_{k=1}^{H} \tilde{a}_k \cos(\omega_{f1} t) + \tilde{b}_k \sin(\omega_{f1} t) \; H \in \mathbb{N}. \tag{3.7}$$

In this example, ω_m and ω_{f2} are super-harmonic of ω_{f_1}, and cause the effect of super-harmonics on the response curve the same as in the previous example (see Figure 3.9(a)). These peaks appear in $\frac{\omega_{f1}}{\omega_n} = 0.5\&0{,}25$, respectively. Again, the peak of the error's curve on $\frac{\omega_{f1}}{\omega_n} = 0.15$ is caused by super-harmonics at $6\omega_{f1}$ (see Figure 3.9(b)). The error can be reduced by including more harmonic terms in Eq. (3.7).

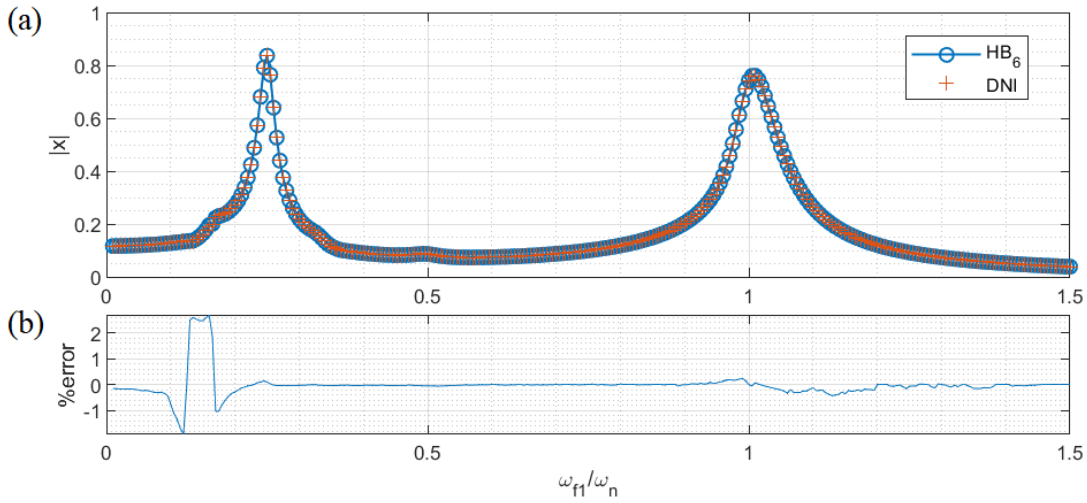

Figure 3.9: The response of HB method has been verified by DNI for linear oscillator under parametric and two external harmonic excitations, (a) comparing the response of DNI by HB continuation method, (b) comparing the response of DNI by HB with zero initial guesses in percentage ($\omega_m = 2\omega_{f1} = 0.5\omega_{f2}$, k_0=1, k_m=0.1, ζ =0.05, F_1=0.05, F_1=0.08).

3.3 Nonlinear Systems Subject to Parametric and External Excitation

In this section, the behavior of FPO's with different types of nonlinearities are studied. The governing equation of this type of motion can be described as the following equation:

$$m\ddot{x} + 2\,\zeta\,\dot{x} + (k_0 + k_m \cos(\omega_m t))x + k_q x^2 + k_c x^3 = F\cos(\omega_f t + \phi) \tag{3.8}$$

where k_q and k_c are the coefficients of the quadratic and cubic nonlinear terms, respectively, and ω_m is equal to multiply integers of ω_f. The primary effect of nonlinearity appears near the resonance frequency. In the absence of damping, nonlinearity prevents the response amplitude from becoming infinite at the resonance frequency. Also, the frequency response curve is bent to the right or left according to the hardening or softening nonlinearity stiffness.

We mainly focus on the effect of cubic nonlinearity on the frequency response of the system ($k_q = 0$). We briefly discuss the influence of quadratic nonlinearity at the end of this section. There are different examples of parametric systems with cubic nonlinearity. The nonlinear micro amplifier tuning on $\omega_m = 2\omega_f$ [40] or vibration model of the horizontal axis wind turbine blade vibration Ref. [39] with the same internal and external excitation frequency, are examples for this type of system.

Figure 3.10 shows the frequency response curve of Eq. (3.8) with hardening cubic nonlinearity. The effect of nonlinearity causes the response to remain bounded while the system parameter is below or above the instability threshold. There is excellent agreement between the HB and the direct time solution in stable points. The two closed ends of the internal loop are shown in insets.

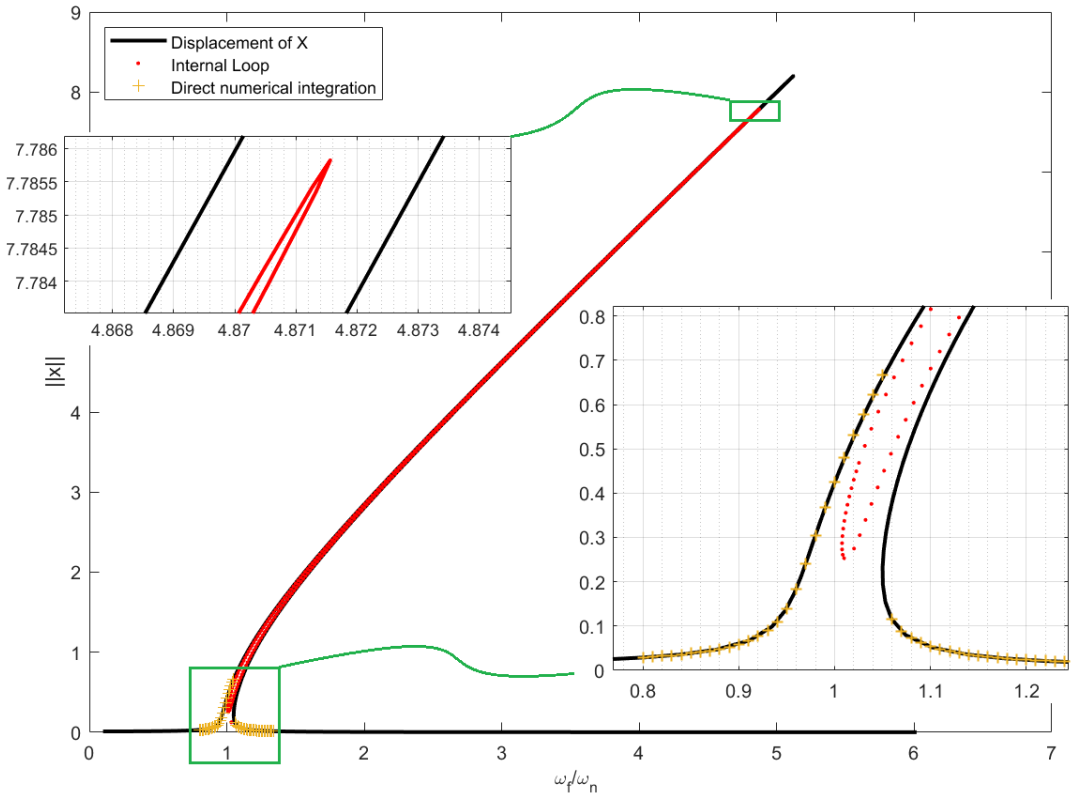

Figure 3.10: Effect of cubic nonlinearity in super-threshold when the modulation frequency equal to two-time excitation one (k_0=1, k_m=0.1, k_c =0.5, ζ =0.005, F=0.01, H=2).

For verifying the result, only the result of the HB method by starts from zero initial guesses illustrated in Figure 3.11(a). Comparing the HB by DNI method shows only the small error that is illustrated in Figure 3.11(b) in percentage. The Super-harmonic resonance is represented on an

external excitation frequency equal to 1/3(rad/s). Figure 3.11(c) presents the comparison between the Fourier Transfers of their results in the time-domain of HB and DNI method. That graph shows the HB method utilizable to predict the steady-state motion of the system in the time domain.

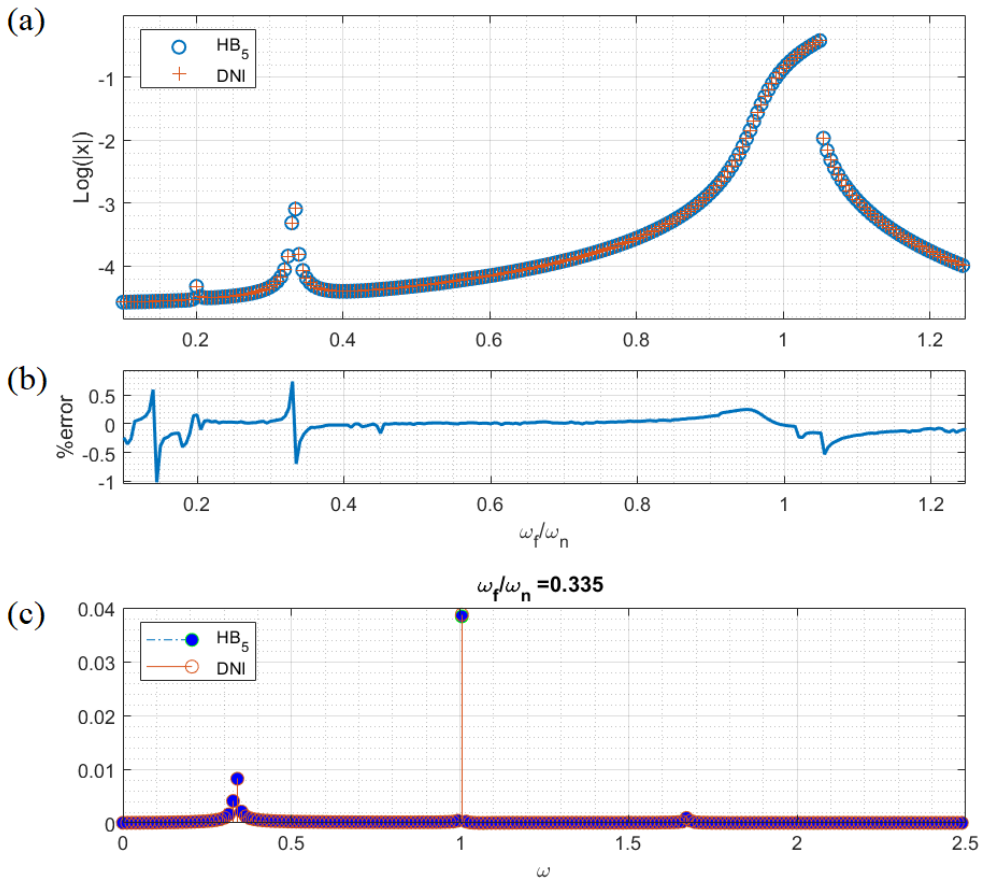

Figure 3.11: Verifying the result of the HB method in nonlinear system by DNI, (a) comparing the response of DNI with HB continuation method, (b) comparing the response of DNI with HB with zero initial guesses in percentage, (c) comparing by FFT in first peak $\omega_f/\omega_n = 1/3$.

As another example, we have chosen $\omega_m = \omega_f$ for Eq. (3.8) such that it represents the horizontal axis wind turbine blade vibration Ref. [39]. The HB method can represent all harmonic and super-harmonic resonances of the blade (see Figure 3.12(a)). The result of the HB method with zero initial guesses are compared in Figure 3.12(b) by the DNI method, in percentage. The error is less than 2 percentage and acceptable for this number of harmonic terms (H=6). Figure 3.12(c) shows the Fourier transfer of result of two methods in the time domain for $\frac{\omega_f}{\omega_n} = 0.5$. This

graph shows the maximum error comes from the difference in the coefficient of primary frequency.

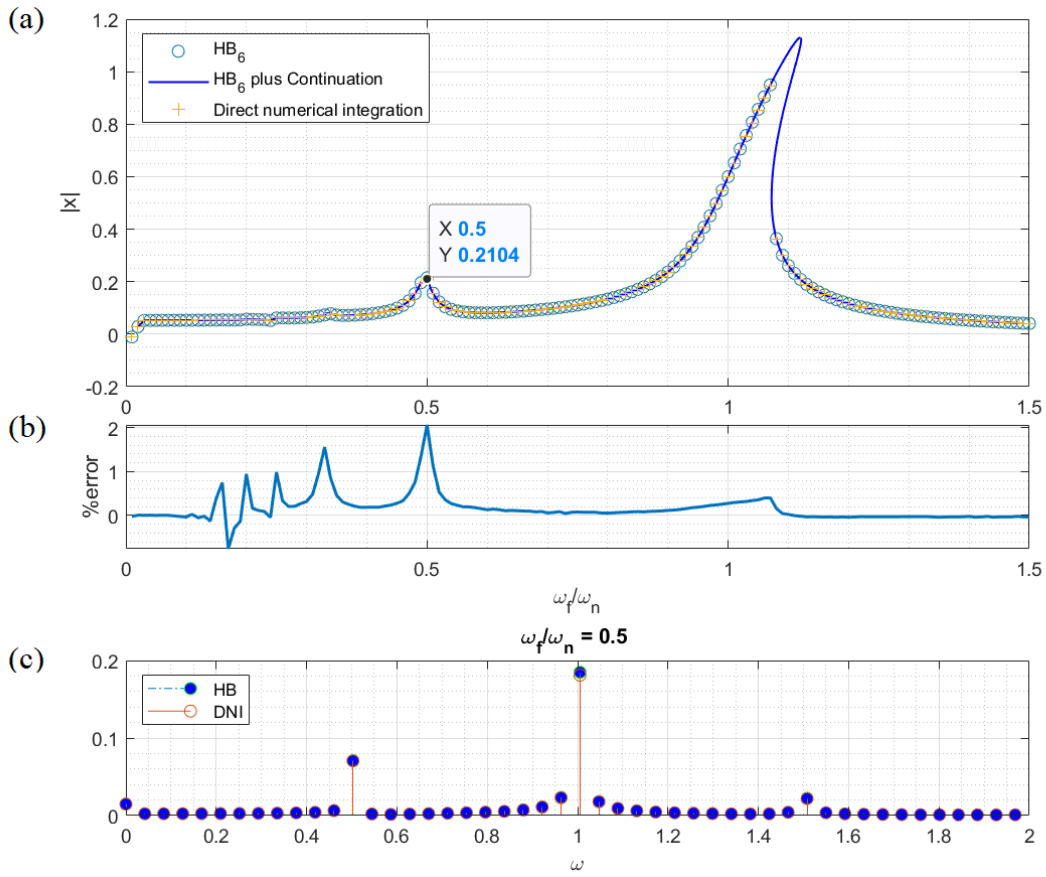

Figure 3.12: (a) Comparing the response of DNI with HB continuation method, (b) comparing the response of DNI with HB with zero initial guesses in percentage, (c) comparing with FFT in $\omega_f/\omega_n = 0.5$ *(*$\omega_m = 2\omega_f$*,* k_0*=1* k_m*=0.3* k_c*=0.3* ζ *=0.025 F=0.05* ϕ*=-*π*/4).*

The HB method could also predict a parametric oscillator's frequency responses subject to two or more harmonic external forces. Assume the Eq.3.6 with cubic nonlinearity and excitation frequencies are harmonic of each other. An example of this problem is illustrated in Figure 3.13 and verifying by DNI method.

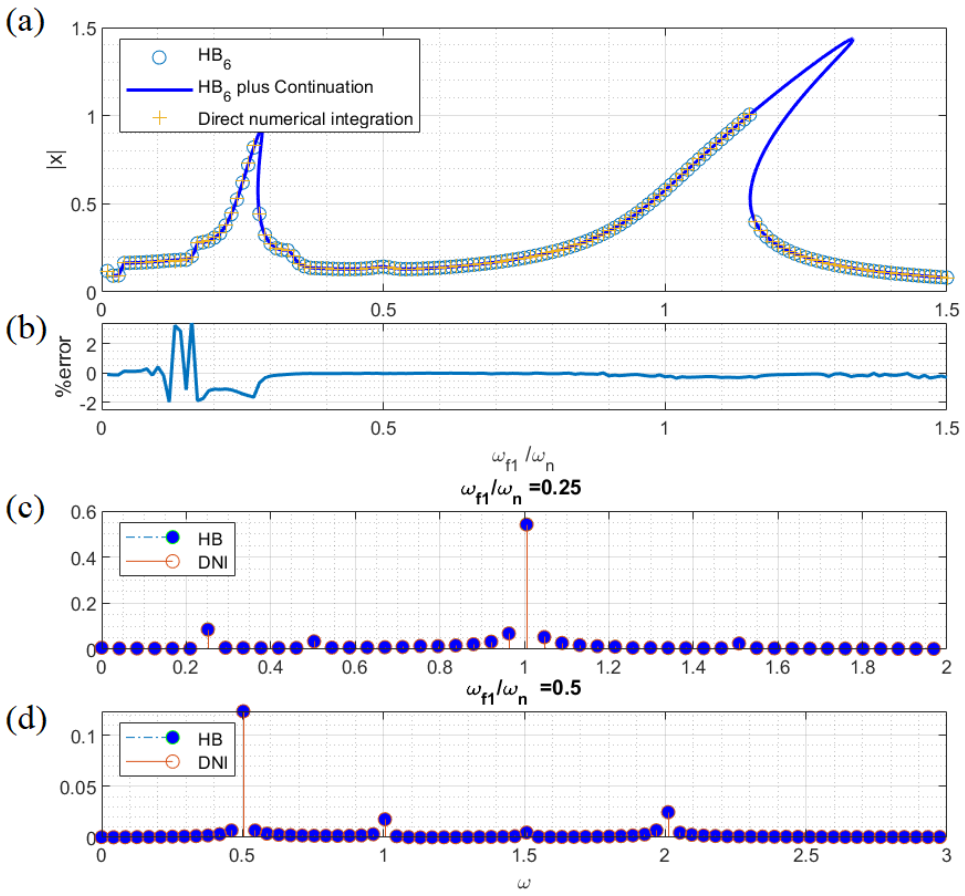

Figure 3.13: The response of HB method for nonlinear oscillator under parametric and two external harmonic excitations (a) comparing the response of DNI with HB continuation method, (b) comparing the response of DNI with HB with zero initial guesses in percentage, (c) comparing by FFT in first peak $\omega_{f1}/\omega_n = 0.25$, (d) comparing with FFT in second peak $\omega_{f1}/\omega_n = 0.5$. ($4\omega_{f1} = 2\omega_m = \omega_{f2}$, k_0=1 k_m=0.1 k_c=0.5 ζ =0.04 F_1=0.1, F_2=0.8).

Analyzing the response of a dynamic system with both cubic and quadratic nonlinearity is more complicated than a system affected by only one of them. The system behavior near the primary resonance is affected by the value of k_c in comparison with k_q [42]. The engineering example of this dynamic motion is a twin-tail aircraft [38]. Figure 3.14 illustrates an example of this system and compares the results with the DNI method. The response shows both hardening and softening effects of quadratic and cubic nonlinearity, respectively. The bottom half of the resonance zone is affected by quadratic nonlinearity and bends to the left, and higher amplitude at that zone is affected by pure cubic nonlinearity and turns to the right. At each turning point, the stability of the system changes that is analyzed in Neumeyer et al.'s work [42].

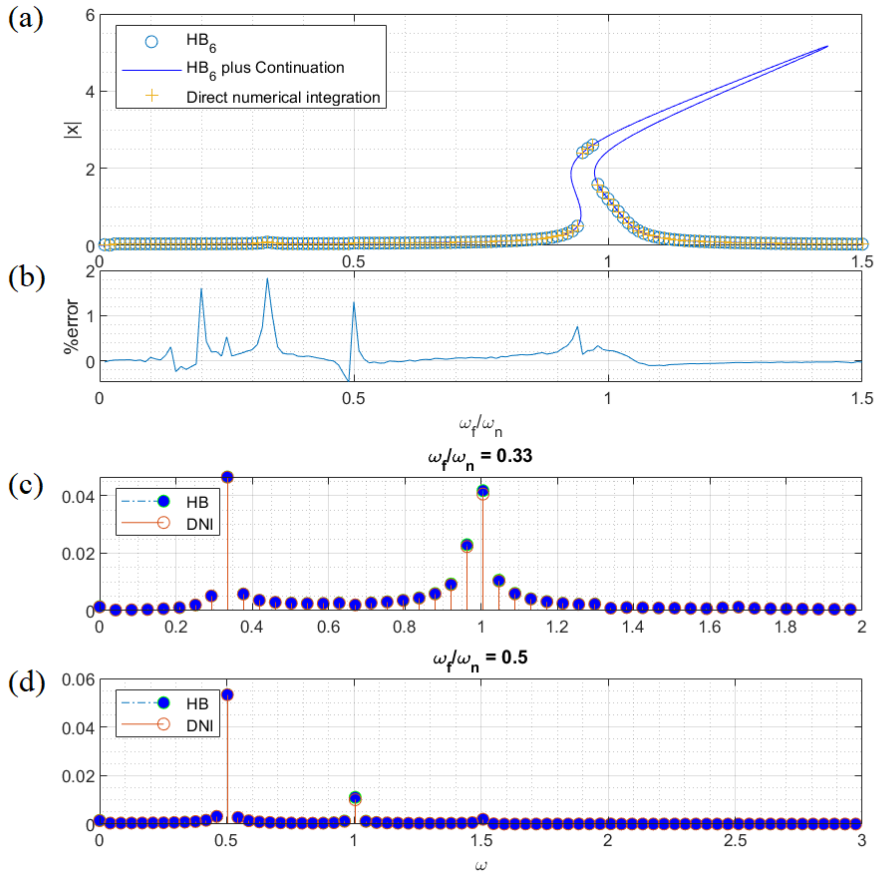

Figure 3.14: The response of HB method verifying by DNI in time and frequency domains for the system with both quadratic and cubic nonlinearities, (a) comparing the response of DNI by HB continuation method, (b) comparing the response of DNI by HB with zero initial guesses in percentage, (c) comparing with FFT in first peak $\omega_f/\omega_n = 0.33$, (d) comparing by FFT in second peak $\omega_f/\omega_n = 0.5$ ($\omega_m = 2\omega_f$, k_0=1 k_m=0.1 k_q=0.3 k_c=0.05 ζ =0.02 F=0.04 ϕ=-π/4).

3.4 Summary

In this Chapter, the HB method was used to study the steady-state response of a system subject to parametric and external excitation. The ratio of the frequencies of the two excitations was fixed to a rational number (2, 3, 1/2). This condition ensures that the steady-state response to be periodic in time. As all response components are harmonic, the Galerkin projection method was used to find the algebraic system of equations required for HB analysis. The AFT method was used for analyzing quadratic and cubic nonlinearity. We analyzed the stable and unstable response of the force parametric oscillator and investigated the effect of nonlinearity on the internal loops appearing in the frequency response curves.

CHAPTER 4 Systems Subject to Parametric and External Excitation: Non-Periodic Oscillations

4.1 Introduction

In this Chapter, we study the steady-state dynamics of a system subject to parametric and external excitations with independent frequencies. Because the frequencies of parametric and external excitation can be incommensurate, the response of the system is no longer periodic. Therefore, a single-frequency Fourier series is no longer a suitable approximation of the response and needs to be updated. The maximum response amplitude is mainly affected by the external force and is independent of the parametric excitation, but the resonance frequency depends on the amplitude of the parametric excitation. There are some combination resonances on the frequency response curve that occur at a frequency equal to the external frequency plus integer multiples of the parametric excitation frequency. The Galerkin projection and AFT method can no longer be used in this case, and a different methodology is needed for HB analysis. Therefore, solving this problem using the HB is not straightforward.

For clarification assume an example of a forced parametric oscillator that is shown in Figure 4.1. What we solved in Chapter 3 covers the frequency response through black lines only, but what will be solved in this Chapter approximates all frequency responses independently to the relation between exaction frequencies. Obtaining the method for solving the system with independent excitation frequencies assists in predicting the behavior of all different types of forced parametric systems, whether the relation between excitation frequency is integer, rational, or irrational number. In this way, the result of this solution can predict the periodic response of the oscillator with dependent frequency excitations as well as the quasi-periodic response of the oscillator with independent frequencies.

In this Chapter, the quasi-periodic motion of the parametric oscillator is analyzed by adjusting the exponential form of HB (AHBM). In this method first, a few points from the response curve are selected. The steady-state response at the selected frequencies is calculated using the DNI method and transferred to the frequency domain to identify the frequency component of the response. This information is used to adjust the HB with a related index. The technique is similar to the Trained harmonic balance method (THBM) [43]. After validating the methodology, the influence of nonlinearity is studied.

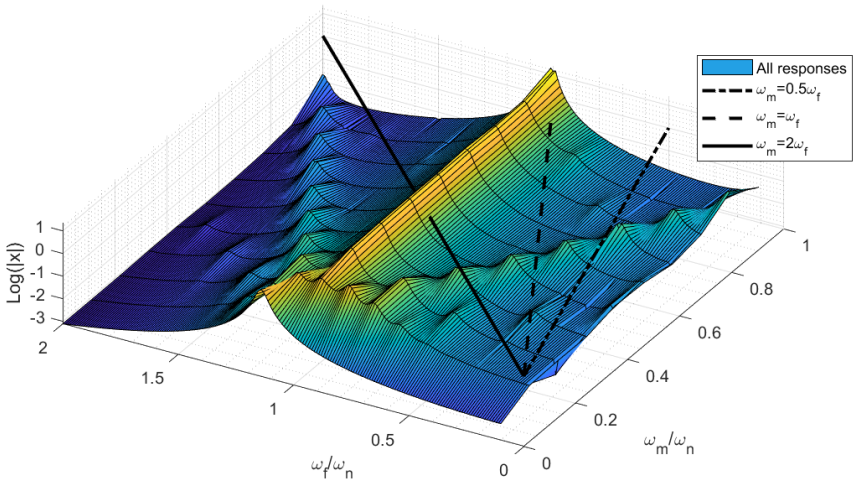

Figure 4.1: An example of all possible responses for Eq. 3.1 (k_0=1 k_m=0.3 ζ =0.025 F=0.12 ϕ=0).

4.2 Systems with one degree of freedom

The motion of a system with parametric and external excitation is described by the following equation:

$$\ddot{x} + 2\zeta\dot{x} + k(t)x = Fcos(\omega_f t - \varphi) \tag{4.1}$$

where ($\dot{}$) denotes temporal derivatives, ζ is the damping ratio, F and ω_f are the direct excitation amplitude and frequency, t is time, φ is the phase difference between the external and parametric excitation and

$$k(t) = k_0 + k_m \cos(\omega_m t + \phi) \tag{4.2}$$

where k_0 stands for stiffness and the $k_m$is the parametric excitation amplitude. The time-dependent stiffness can be rewritten in complex Fourier series form:

$$k(t) = \sum_{p=-\infty}^{\infty} \hat{k}_p e^{ip\omega_m t} \tag{4.3}$$

where $\hat{k}_p$ is defined as:

$$\hat{k}_p = \frac{\omega_m}{2\pi} \int_{-\frac{\pi}{\omega_m}}^{\frac{\pi}{\omega_m}} k(t)\, e^{-ip\omega_m t} dt. \tag{4.4}$$

The only Fourier coefficients are, $\hat{k}_0 = k_0$, $\hat{k}_{+1} = \frac{k_m e^{i\phi}}{2}$ and $\hat{k}_{-1} = \frac{k_m e^{-i\phi}}{2}$. All the coefficients with an index larger than one ($|p| > 1$) are equal to zero. For applying the AHBM, four points from an example direct integration frequency response curve are selected. This selection includes a local minimum in low frequency and three main peaks of the steady-stead frequency response of the system (see Figure 4.2). Responses of the system in selected points are then transferred to the frequency domain to define the frequency components. The dominant frequencies are the external excitation frequency (ω_f) and the multiple integers of parametric excitation frequency plus the external one ($\omega_f \pm \omega_m$). This result is the same as what we expected from the theoretical solution (see Appendix B). Therefore, the answer can be assumed as:

$$X(t) = \sum_{n=-h}^{h} a_n \cos(\omega_f + n\omega_m) + b_n \sin(\omega_f + n\omega_m). \tag{4.5}$$

which can be rewritten in the complex notation as:

$$U(t) = \left(\sum_{n=-\infty}^{\infty} \widehat{U}_n e^{in\omega_m t} \right) e^{i\omega_f t}, \tag{4.6}$$

$$\widehat{U}_n = a_n + ib_n, \tag{4.7}$$

The governing equation Eq. (4.1) can therefore be transformed into a system of algebraic equations for the unknown amplitudes like:

$$\left(-m \begin{bmatrix} (\omega_f - \omega_m)^2 & 0 & 0 \\ 0 & \omega_f^2 & 0 \\ 0 & 0 & (\omega_f + \omega_m)^2 \end{bmatrix} + ic \begin{bmatrix} (\omega_f - \omega_m) & 0 & 0 \\ 0 & \omega_f & 0 \\ 0 & 0 & (\omega_f + \omega_m) \end{bmatrix} + \begin{bmatrix} \hat{k}_0 & \hat{k}_{-1} & 0 \\ \hat{k}_{+1} & \hat{k}_0 & \hat{k}_{-1} \\ 0 & \hat{k}_{+1} & \hat{k}_0 \end{bmatrix} \right) \begin{bmatrix} \widehat{U}_{-1} \\ \widehat{U}_0 \\ \widehat{U}_{+1} \end{bmatrix} = \begin{bmatrix} 0 \\ F \\ 0 \end{bmatrix}. \tag{4.8}$$

By separating Eq. (4.8) into the real and imaginary parts and solving them together, the coefficient of the Fourier series will be obtained. Figure 4.3(a) shows a good agreement between AHBM and the result of the DNI method. The lower frequencies are represented in the inset to show the effect of harmonic excitation on the response of the system. Every time $\omega_m = n\omega_f (n \in 2\mathbb{N})$, the response becomes harmonic and falls to a lower amplitude. After passing through each of these points, the rate between frequencies becomes irrational again and the response becomes quasi-periodic, the amplitude rises sharply and reaches the previous value. Additionally, local minimums in the response amplitude are observed at linear combinations of these frequencies. An example of

this periodic response in the local minimums is shown in the time domain by the DNI method as the first point of Figure 4.2 ($\omega_m/\omega_n = 2\omega_f/\omega_n = 0.3$). If excitation frequencies are locked at this rate, without any change in Eq. (4.8), the AHBM can show the response of a perfect tuning amplifier the same as Figure 3.2. We can repeat this calculation for all other linear results of the previous Chapter.

Figure 4.4 shows that the location and value of the local minimum of the frequency response curve depend on the phase difference between the external and parametric excitations (φ). Increasing the phase from zero to $\frac{\pi}{2}$ splits the local minimum into two smaller ones. Consequently, if we decided to use this frequency as an amplifier the larger φ give as a bigger amplitude but as a filter $\varphi = 0$ is the best.

There are some errors in the approximate solution that depends on the number of terms used in the assumption. Figure 4.3(b) shows how including more terms in Eq. (4.5) can decrease the error of our approximation. The fluctuation in error percentage after 1.2 and before 0.8 shows that the two first approximate responses of HB are not acceptable far from the primary resonance frequency. These errors are caused by terms with a higher harmonic of the parametric excitation frequency. Figure 4.5 shows the FFT of the response on a logarithmic scale in the range of $\omega_f/\omega_n = [0,2]$ from direct time integration. A large value of k_m near the stability threshold of the system is selected for a better illustration of the effect of terms with higher harmonics of ω_m (the dominant frequencies of response). The graph shows an increasing in that effect in lower excitation frequencies. This illustration explains why the terms with higher harmonics of ω_m (as example $h \geq 3$ for $\omega_m/\omega_n \geq 1/3$) must be included in our assumption while they are out of the investigated frequency range. An example of including negative frequencies like ($\omega_f - n\omega_m : n \in \mathbb{N}$ & $\omega_f < n\omega_m$) in the Fourier expansion of the response is shown in Figure 4.6 with red arrows.

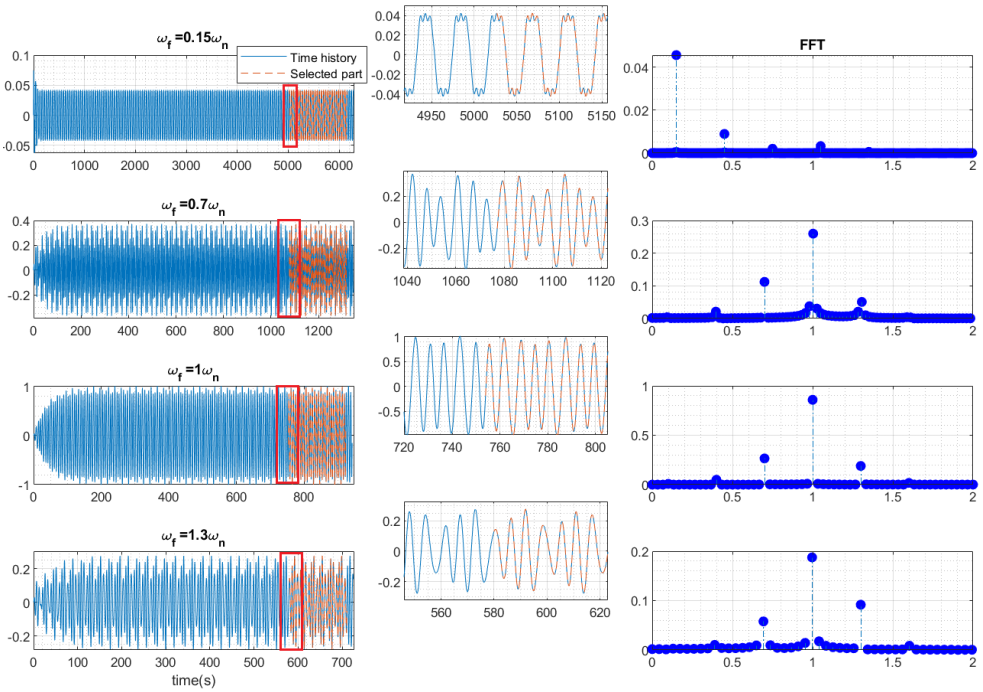

Figure 4.2: Time history and frequency spectrum at four external frequencies. The corresponding frequency response curve is shown in Figure. 4.3(a).

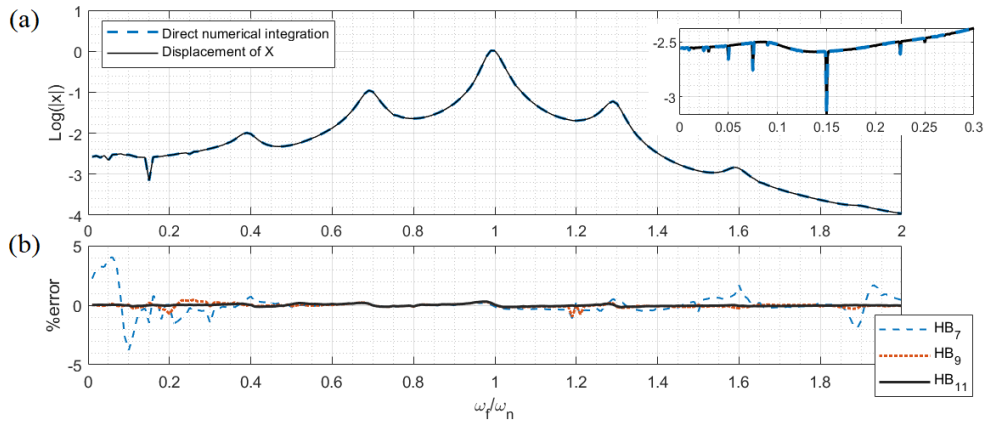

Figure 4.3: Comparing the exponential HB with DNI (a) in frequency domain and (b) the error percentages of different number of harmonic terms ($\omega_m = 0.3, \zeta = 0.025, k_m = 0.3, F = 0.05$).

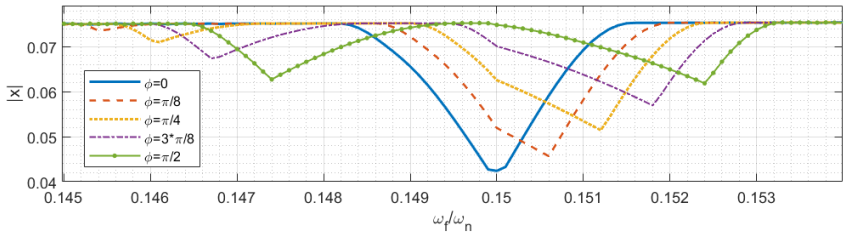

Figure 4.4: Effect of changing the phase between the external and parametric excitation on local minimum ($\omega_m = 0.3, \zeta = 0.025, k_m = 0.3, F = 0.05$).

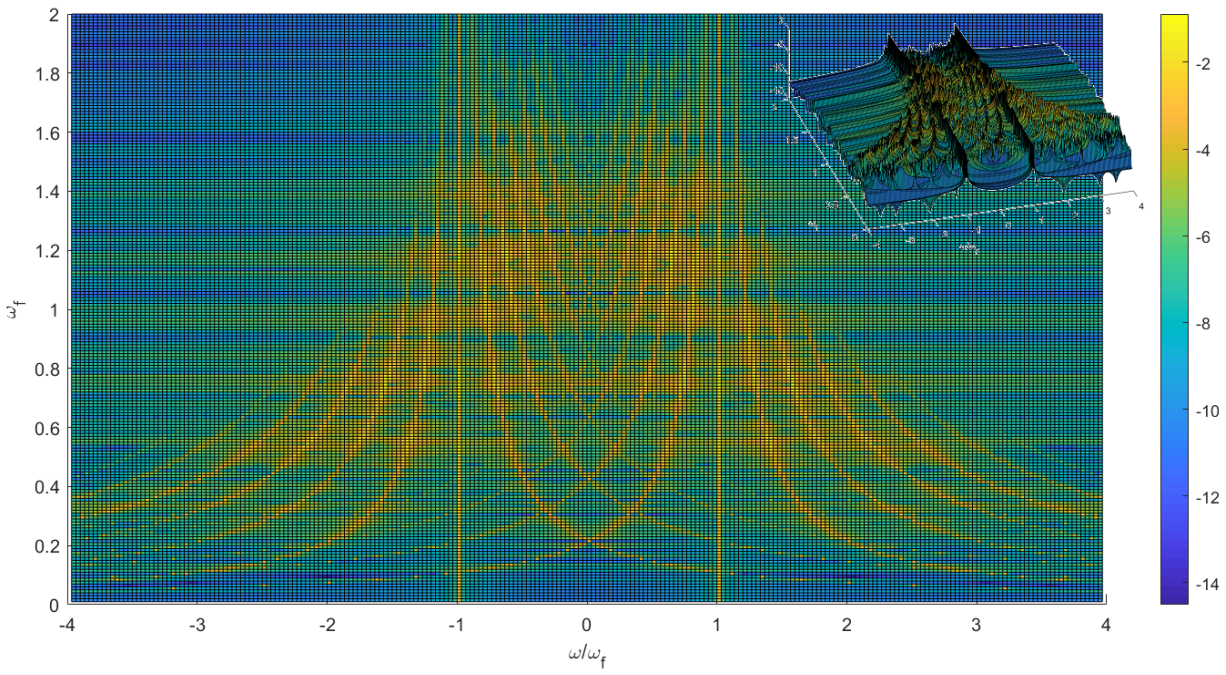

Figure 4.5: The FFT of DNI response in different external excitation frequencies in logarithmic view. The result of FFT is nondimensionalized by dividing the response frequency to ω_f. The 3D view of this graph was represented on the inset ($\omega_m = 0.21$, $\zeta = 0.025, k_m = 0.7, F = 0.05$).

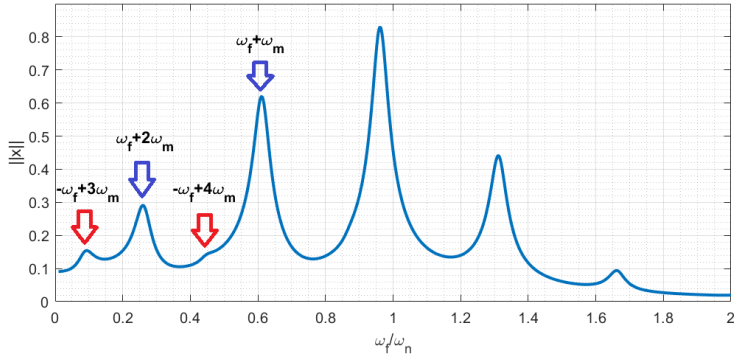

Figure 4.6: Effect of two negative frequencies in response curve. This effect also discuss in Kaijun et al. work [44] *($\omega_m = 0.35$, $\zeta = 0.025, k_m = 0.7, F = 0.05$).*

Figure 4.6 shows a resonance near the natural frequency of the non-parametric system. This frequency can be assumed as an approximate natural frequency (ANF) for the system. The value of this ANF depends on the parametric excitation amplitude. Comparing this figure with the previous result shows increasing the value of k_m causes to shift of all peaks of the frequency response curve to the lower frequencies. Figure 4.7(a) shows this shift in primary resonance in the range $k_m = [0\ 0.6]$. Increasing the value of k_m has the same effect on other peaks of the frequency response curve. Another effect of k_m, which appears in the large value of it, is the unstable behavior of the system. Figure 4.7(b) presents an example of this instability in the time

domain. The onset of this instability depends on the values of the damping coefficient and the parametric excitation frequency, but this critical value is independent of the external force because the system is linear, and the numerical response of the free oscillator shows the same onset for instability.

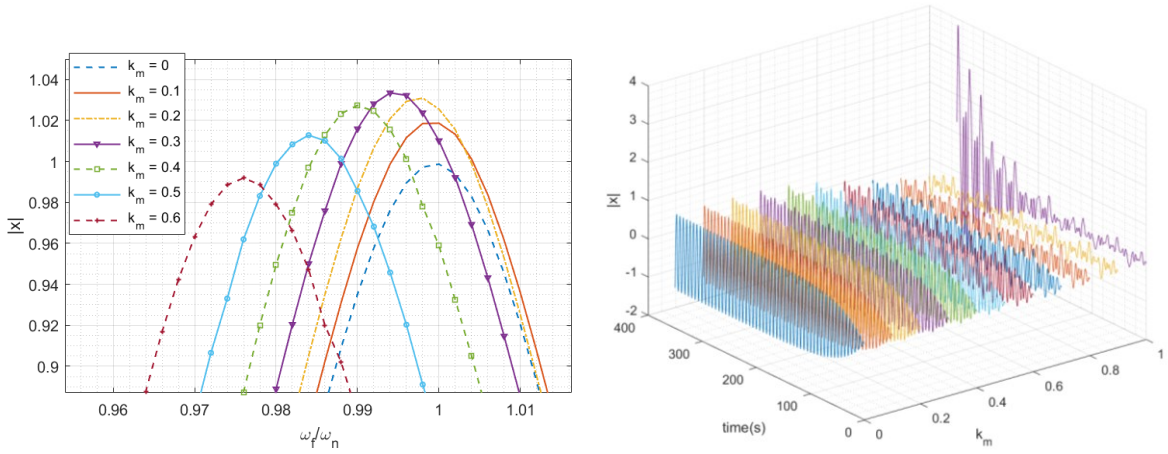

Figure 4.7: The effect of increasing k_m, (a) on resonance frequency, (b) on stability (solved by DNI, $\omega_m = 0.3, \zeta = 0.025, F = 0.05$).

4.2.1 Stability of linear oscillations

Some combinations of parameters can lead to instabilities in the response of the system, as shown in Figure 4.7(b). In this section, regions of the parametric excitation parameters are determined where the response remains stable. Our analysis of stability is based on the free response of the system. This is because the external force does not influence the onset of instability in a linear system. We have verified this claim numerically.

The governing equation is nondimensionalized:

$$\frac{d^2x}{d\tau^2} + \bar{c}\frac{dx}{d\tau} + (\delta + \epsilon\cos\tau)\,x = 0, \tag{4.9}$$

where the new variables are

$$\tau = \omega_m t,\ \bar{c} = 2\zeta\frac{\omega_n}{\omega_m},\ \delta = \frac{\omega_n^2}{\omega_m^2},\ \epsilon = \frac{k_m}{k_0}\frac{\omega_n^2}{\omega_m^2}. \tag{4.10}$$

By defining $x_1 = x$ and $x_2 = dx/d\tau$, Eq. 4.9 is solved for the two different initial conditions:

$$\begin{bmatrix} x_{11}(\tau) \\ x_{12}(\tau) \end{bmatrix}_{\tau=0} = \begin{bmatrix} 1 \\ 0 \end{bmatrix}, \qquad \begin{bmatrix} x_{21}(\tau) \\ x_{22}(\tau) \end{bmatrix}_{\tau=0} = \begin{bmatrix} 0 \\ 1 \end{bmatrix}. \tag{4.11}$$

The system is stable if [45]:

$$\left| Tr \begin{bmatrix} x_{11}(\tau) & x_{21}(\tau) \\ x_{12}(\tau) & x_{22}(\tau) \end{bmatrix}_{\tau=2\pi} \right| < 2. \tag{4.12}$$

The result of this computation is shown in Figure 4.8 for different values of the damping.

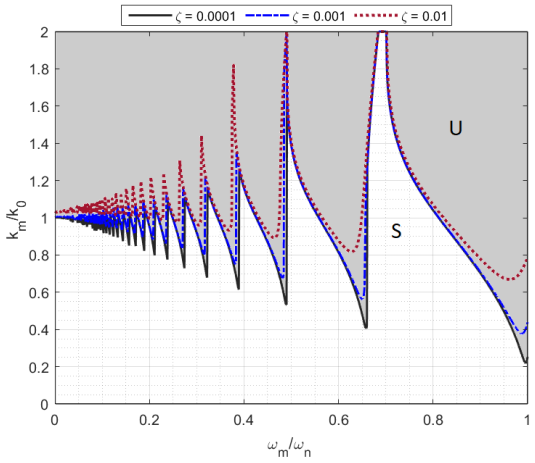

Figure 4.8: The stability diagram, as a function of the modulation parameters for different damping ratios.

4.2.2 Influence of nonlinearity

In this section, we add a nonlinear stiffness term to Eq. (4.1):

$$\ddot{x} + 2\zeta\dot{x} + (k_0 + k_m \cos(\omega_m t + \phi))x + \alpha x^3 = F\cos(\omega_f t - \varphi), \tag{4.13}$$

where α denotes the coefficient of the nonlinear term. When the excitation frequencies vary independently, the response becomes non-harmonic in most situations. As a result, the AFT method can no longer be used for the nonlinear problem. The AFT method is based on inverse Fourier transfer that is only applicable to harmonic function. Therefore, we use the AHBM without Galerkin projection, the AFT method, and the Fourier series's exponential form with a procedure explained in Appendix(D). According to the FFT of time response of the system (Figure 4.9) and especially near the primary resonance frequency (see Figure 4.10), an assumption for the displacement of the system with seven terms is:

$$\begin{aligned} X_1 = {} & A_1 \cos(\omega_f t) + B_1 \sin(\omega_f t) + A_2 \cos((\omega_f - \omega_m)t) + B_2 \sin((\omega_f - \omega_m)t) \\ & + A_3 \cos((\omega_f + \omega_m)t) + B_3 \sin((\omega_f + \omega_m)t) \\ & + A_4 \cos((\omega_f - 2\omega_m)t) + B_4 \sin((\omega_f - 2\omega_m)t) \\ & + A_5 \cos((\omega_f + 2\omega_m)t) + B_5 \sin((\omega_f + 2\omega_m)t) \\ & + A_6 \cos((\omega_f - 3\omega_m)t) + B_6 \sin((\omega_f - 3\omega_m)t) \\ & + A_7 \cos((\omega_f + 3\omega_m)t) + B_7 \sin((\omega_f + 3\omega_m)t). \end{aligned} \tag{4.14}$$

Substituting Eq. (4.14) into Eq. (4.13) and balancing the harmonic terms (see Appendix D) results in a system of algebraic equations in terms of the unknown amplitudes. Figure 4.11 compares the result of the solution with DNI. There is an excellent agreement with the DNI at the selected points except at $\omega_f/\omega_n = 1.17$. The FFT of the time-domain response at this frequency shows frequencies equal to $\omega_f \pm \frac{n\omega}{2}$ are the main reason for this peak (see Figure 4.12(b)). Unfortunately, adding $\omega_f \pm \omega_m/2$ to the Eq. (4.14) did not decrease the error, and the coefficients related to these frequencies are almost zero in all different external frequencies. However, the maximum amplitude at this point can be controlled by changing the value of k_m, as is shown in Figure 4.12(c). Therefore, the AHBM can predict the behavior of the system with a small value of k_m in all frequencies and an extensive range of nonlinearity (see Figure 4.13). The nonlinearity affects the shape of the response curve in the primary resonance and other response peaks. Therefore, it is possible to have five responses in some of the excitation frequencies with large nonlinearity. For example, assuming the $\alpha = 0.9$, there are three stable responses and two unstable in the range of $\omega_f/\omega_n = [1.3,1.332]$ (see Figure 4.13).

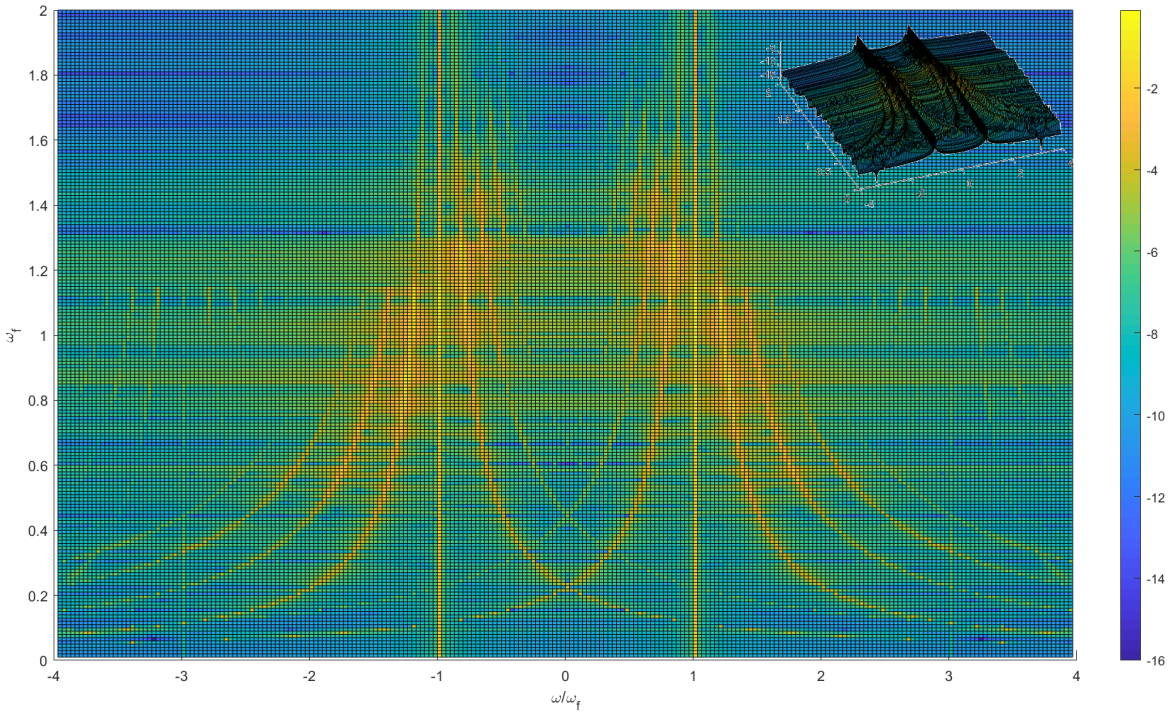

Figure 4.9: The nondimensionalized FFT of DNI response in different external excitation frequencies by the logarithmic view. The jump phenomenon appears in $\omega_f = 1.14$ because all points have zero initial guess. The 3D view of this graph was represented on the inset ($\omega_m = 0.22, k_m = 0.3\ \zeta = 0.025,\ F = 0.12$).

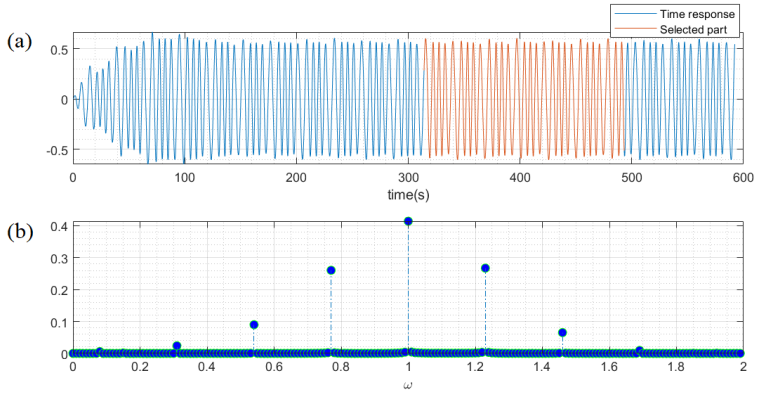

Figure 4.10: The time response and Fourier transfer of nonlinear system in primary resonance frequency ($\omega_f/\omega_n = 1,\ \omega_m = 0.23, k_m = 0.5\ \zeta = 0.025,\ F = 0.05, \alpha = 0.3$).

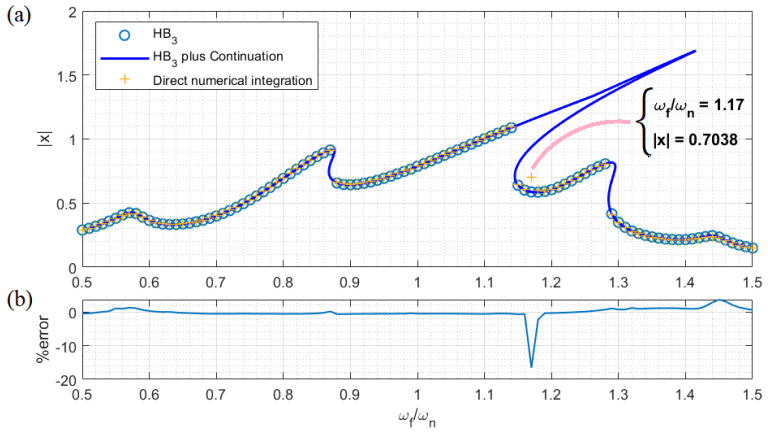

Figure 4.11: The result of applying the HB to nonlinear system with fixed parametric frequency. (a) comparing the frequency response with DNI method ($\alpha = 0.5$)*, (b) the error percentage* ($\omega_m = 0.22, k_m = 0.3, \zeta = 0.025,\ F = 0.12, \alpha = 0.5$).

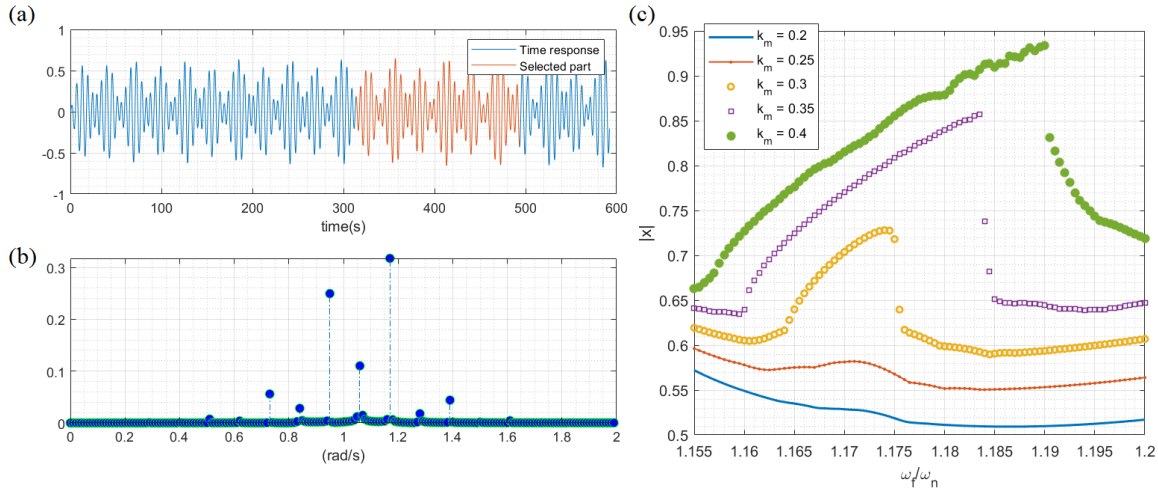

Figure 4.12: (a) the time response and Fourier transfer of the peak at $\frac{\omega_f}{\omega_m} = 1.17, k_m = 0.3$ *and (b) the FFT of this. (c) is effect of changing* k_m *on this point* ($\omega_m = 0.22, \zeta = 0.025,\ F = 0.12, \alpha = 0.5$).

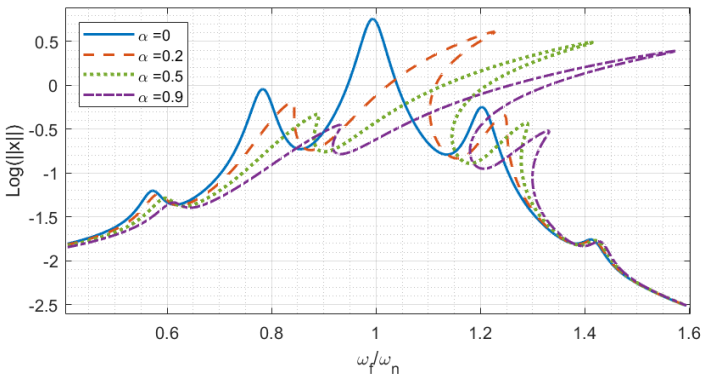

Figure 4.13: The effect of large nonlinearity ($\omega_m = 0.21, k_m = 0.3,\ \zeta = 0.025,\ F = 0.12$).

4.3 Systems with multiple degrees of freedom

In this section, responses of systems with more than one degree of freedom are investigated. According to the AHBM methodology, in each case, a few points of the frequency response curve are selected to determine the required frequencies for applying the HB method. Firstly, the two degrees of freedom system is studied, then the verified technique is used to predict the behavior of a non-reciprocal system with two or more degrees of freedom.

4.3.1 Applying the HB method to Two-Degree-of-Freedom forced parametric system

We consider the following system for our computations in this section:

$$m_1\ddot{x}_1 + (c_1 + c_2)\dot{x}_1 - c_2\dot{x}_2 + (k_1 + k_2)x_1 - k_2x_2 = Fcos(\omega_f t) \tag{4.15}$$

$$m_2\ddot{x}_2 - c_1\dot{x}_1 + c_2\dot{x}_2 - k_2x_1 + k_2x_2 = 0 \tag{4.16}$$

$$k_1 = k_{01} + k_{m_1}\cos(\omega_{m_1}t) \tag{4.17}$$

$$k_2 = k_{02} + k_{m_2}\cos(\omega_{m_2}t) \tag{4.18}$$

where $\omega_{m_1} = 0.3$ and $\omega_{m_2} = 0.25$ as a representative example. The governing equations are solved using the DNI method in the time domain at a frequency near the first primary resonance (see Figure 4.14(a)), then the steady-state part of the result is transferred to the frequency domain by FFT to find all frequencies in the response curve (see Figure 4.14(b)).

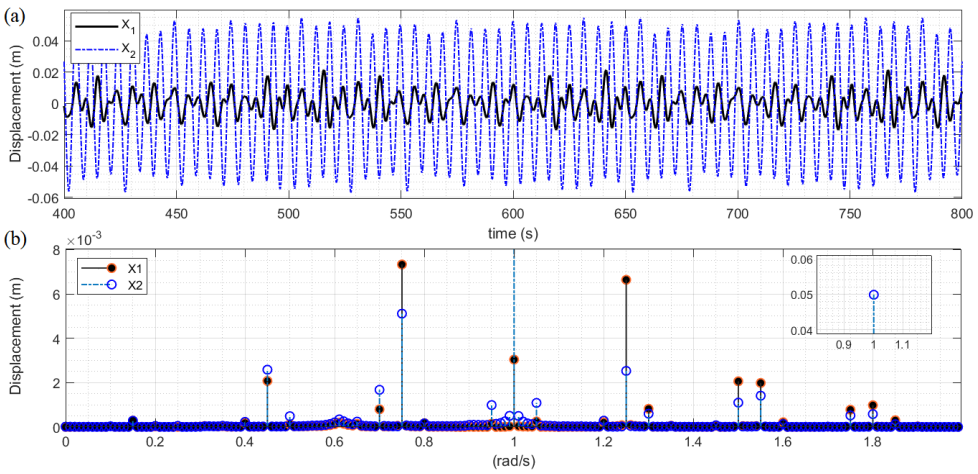

Figure 4.14: (a) The response of oscillation in time domain for $\omega_f/\omega_n = 1$, (b) the result of transferring the steady-state response to frequency domain.($\omega_{m1} = 0.3, \omega_{m2} = 0.25, k_0 = 1, k_{m1} = 0.3, k_{m2} = 0.2, c_1 = c_2 = 0.05,\ F = 0.05$).

According to the result, the dominant frequencies are:

$X_1: \omega_f - \omega_{m_2},\ \omega_f + \omega_{m_2},\ \omega_f,\ \omega_f - \omega_{m_2} - \omega_{m_1},\ \omega_f + 2\omega_{m_2}\ ,\ \omega_f - \omega_m,\ \omega_f + \omega_{m_2} + \omega_{m_1}, \omega_f + 2\omega_{m_2} + \omega_{m_1}, \omega_f + 2\omega_{m_1}, \omega_f - 2\omega_{m_1}, \omega_f - 3\omega_{m_2}, \omega_f + \omega_{m\_2} + 2\omega_{m_1}\ \ldots$

$X_2: \omega_f,\ \omega_f - \omega_{m_2},\ \omega_f + \omega_{m_2},\ \omega_f - \omega_{m_2} - \omega_{m_1},\ ,\ \omega_f - \omega_{m_1},\ \omega_f + \omega_{m_2} + \omega_{m_1},\ \omega_f + 2\omega_{m_2}, \omega_f - \omega_{m_2} + \omega_{m_1}, \omega_f + \omega_{m_2} - \omega_{m_1}, \omega_f + \omega_{m_1}, \omega_f + 2\omega_{m_2} + \omega_{m_1},\ \omega_f - 3\omega_{m_2}, \omega_f - 2\omega_{m_1}, \ldots$

Assuming $\omega_{m_2} = \omega_{m_1} = 0.3$ and selecting the first three dominant frequencies, $X_1$and X_2 are expressed as:

$$\begin{aligned} X_1 = {} & A_1 \cos(\omega_f t) + B_1 \sin(\omega_f t) + A_2 \cos((\omega_f - \omega_m)t) + B_2 \sin((\omega_f - \omega_m)t) \\ & + A_3 \cos((\omega_f + \omega_m)t) + B_3 \sin((\omega_f + \omega_m)t) \\ & + A_4 \cos((\omega_f - 2\omega_m)t) + B_4 \sin((\omega_f - 2\omega_m)t) \\ & + A_5 \cos((\omega_f + 2\omega_m)t) + B_5 \sin((\omega_f + 2\omega_m)t), \end{aligned} \tag{4.19}$$

$$\begin{aligned} X_2 = {} & C_1 \cos(\omega_f t) + D_1 \sin(\omega_f t) + C_2 \cos((\omega_f - \omega_m)t) + D_2 \sin((\omega_f - \omega_m)t) \\ & + C_3 \cos((\omega_f + \omega_m)t) + D_3 \sin((\omega_f + \omega_m)t) \\ & + C_4 \cos((\omega_f - 2\omega_m)t) + D_4 \sin((\omega_f - 2\omega_m)t) \\ & + C_5 \cos((\omega_f + 2\omega_m)t) + D_5 \sin((\omega_f + 2\omega_m)t). \end{aligned} \tag{4.20}$$

Substituting this assumption in Eq. (4.15) and Eq. (4.16) gives us the system of equations that predicts the steady-stead response of the system (see Figure 4.15(a)). An excellent agreement of AHBM with DNI is shown in Figure 4.15(b). Adding the second mass changes the shape of the frequency response curve by adding a second set of peaks and relocating the first ANF. The prominent peaks of Figure 4.15(a) are near the natural frequencies of a non-parametric oscillator ($\omega_n = \sqrt{(3 \pm k_0\sqrt{5})/2}$ =1.618,0.618). There are four more small peaks in the frequency response curve of both masses. These peaks located before and after each ANF's near frequency equal to $\omega_n \pm \omega_m$. These secondary peaks are before $\omega_f = 0.318$ and 0.918 for the first ANF and before $\omega_f = 1.318$ and 1.918 for the second. Moreover, there is another peak near the zero frequency before the $\omega_f - 2\omega_m$ ($\omega_f = 0.018$). There are some minimums on super-harmonics of parametric excitation frequency ($\frac{\omega_m}{2}, \frac{\omega_m}{4}, \frac{\omega_m}{6}, \dots$) and linear combinations of them shown in the inset of Figure 4.15(a). At these frequencies, parametric excitation is equal to the even multiple of an external frequency, and therefore the response is periodic.

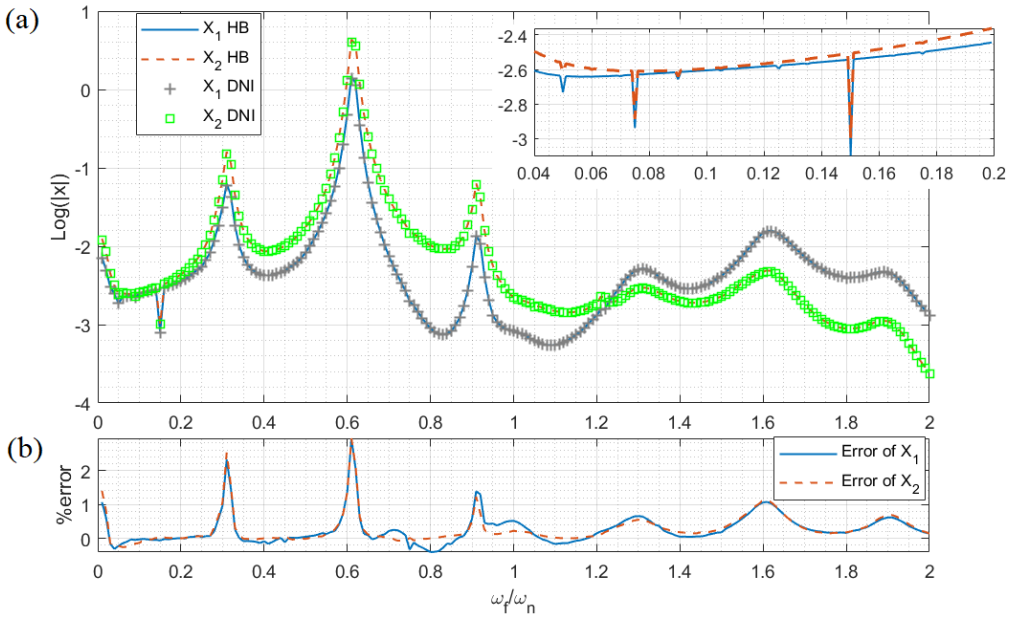

Figure 4.15: The response of HB method is verified by DNI in the frequency domain for two degrees of freedom linear oscillator under parametric and an external harmonic excitation, (a) comparing the frequency response of DNI with HB method, (b) comparing them in percentage ($\omega_m = 0.3, k_m = 0.3, \zeta = 0.025,\ F_1 = 0.05$).

4.3.2 Case study: Reciprocity test in forced parametric system

As a case study, we investigate the response of a system with 2 degrees of freedom in more detail. Specifically, we study the influence of parametric excitation on the reciprocity invariance.

The principle of reciprocity states that wave propagation between two points in an elastic material remains the same when source and receiver are interchanged [46]–[48]. Recently, breaking reciprocity has been explored to create elastic and acoustic wave devices that exploit unidirectional transmission. The general aim is to develop devices and materials that allow the propagation of elastic waves in one direction but not the opposite direction.

Reciprocity holds in linear, time-invariant systems. One way to break the reciprocity invariance a linear system is to modulate the elastic properties of the system [49]. Modulated waveguides are typically modeled as an infinite series of Mathieu equations, which are then analyzed asymptotically in the limit of weak parametric excitation. Recent experimental realizations of modulated waveguides in mechanical systems show they operate beyond these limits. To bridge this gap between the operating regimes of theory and experiments, we study the nonreciprocal dynamics of coupled Mathieu equations at moderate excitation levels using the HB method. We discuss the role of the phase difference between adjacent oscillators, and the influence of nonlinearity on the nonreciprocal bias of the system.

Consider a Multi-Degree-of-Freedom system with external and parametric excitations, as depicted in Figure 4.16. The simple equations of motion for the multidimensional system with independent external and parametric excitation's frequencies are given by:

$$m_1\ddot{x}_1 + 2c\dot{x}_1 - c\dot{x}_2 + (k_1 + k_2)x_1 - k_2x_2 = f_1 cos(\omega_f t) \tag{4.21}$$

$$\vdots$$

$$m_i\ddot{x}_i + c_i(\dot{x}_i - \dot{x}_{i-1}) - c_{i+1}(\dot{x}_{i+1} - \dot{x}_i) + k_i(x_i - x_{i-1}) - k_{i+1}(x_{i+1} - x_i) = 0 \tag{4.22}$$

$$\vdots$$

$$m_n\ddot{x}_n - c\dot{x}_{n-1} + 2c\dot{x}_n - k_nx_{n-1} + (k_n + k_{n+1})x_n = f_n cos(\omega_f t) \tag{4.23}$$

$$k_1 = k_0 + k_p \cos(\Omega_m t - \varphi_1) \tag{4.24}$$

$$k_{n+1} = k_0 + k_p \cos(\Omega_m t - \varphi_2) \tag{4.25}$$

where m stands for mass, c is the damping ratio, f and ω stand for direct excitation amplitude and frequency, t is time, k_0 stands for stiffness and the k_p is the parametric excitation amplitude.

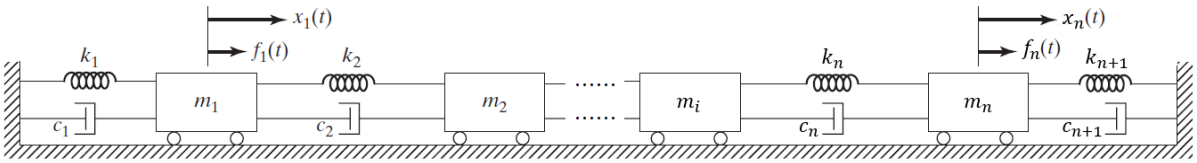

Figure 4.16: A multi-degree-of-freedom system with external and parametric excitations

These equations can be nondimensionalized by dividing to k_0, that yield for example in two degrees of freedom as:

$$\ddot{y}_1 + 4\zeta\dot{y}_1 - 2\zeta\dot{y}_2 + (1 + k_c + k_m\cos(\omega_m\tau - \phi_1))y_1 - k_c y_2 = F_1 cos(\omega_f\tau) \qquad (4.26)$$

$$\mu\ddot{y}_2 + 4\zeta\dot{y}_2 - 2\zeta\dot{y}_1 + (1 + k_c + k_m\, cos(\omega_m\tau - \phi_2))y_2 - k_c y_1 = F_2 cos(\omega_f\tau) \qquad (4.27)$$

where $\omega_0^2 = \frac{k_0}{m_1}$ is a neutral frequency of the unforced system (a simple free vibration system without parametric excitation). The ζ is the damping ratio for the unforced vibration equal to $\frac{c}{2\omega_0 m_1}$ and $\mu = \frac{m_2}{m_1}$. The new nondimensional time scale τ is equal to $\omega_0 t$. Assuming $y_1$and y_2 the same as $X_1$and X_2 at Eq. (4.19) and Eq. (4.20), respectively. The following values are chosen for the system parameters in this section:

$$k_c = 1.5, k_m = 0.2, \mu = 1, \omega_m = 0.23, \zeta = 0.008, \phi_1 = \phi_2 = 0.$$

The system is solved in two opposite directions. In the first case, the second mass is selected as the source and excited by a periodic external force ($F_1 = 0, F_2 = 1$) and the first mass assumed as the receiver. Then for studying the reciprocity effect, we swap the source and receiver by changing the force location ($F_1 = 1, F_2 = 0$). The first case is shown by a superscript (i), and the second is shown by a superscript (ii). If the responses of the two receivers are identical, then we say that the response is reciprocal. We expect a reciprocal behavior for the system described by Eqs. (4.26) and (4.27) when there is no phase difference between the parametric excitations applied to the two masses ($\phi_1 = \phi_2$).

The frequency response curve that is presented in Figure 4.17(a) has several maximums and minimums. The main peaks occur near the natural frequencies of a non-parametric oscillator ($\omega_1 = \sqrt{k_0/m} = 1\ and\ \omega_2 = \sqrt{1 + 2K_c} = 2$). There are several smaller peaks near $\omega_n \pm \omega_m$ in $\omega_f/\omega_n = 0.77$ and 1.23 for the first ANF and $\omega_f/\omega_n = 1.77$ and 2.23 for the second ANF. Other important peaks of this curve appear near the $\omega_n \pm n\omega_m$ ($n = 2,3,4$ ...). The system's antiresonant

frequency appears between the two ANFs ($\omega_f/\omega_n = 1.6$). The results of the HB method for both cases are validated by DNI. Figure 4.17(b) shows the excellent agreement of result with DNI. The error of the HB method in this example is less than 1%.

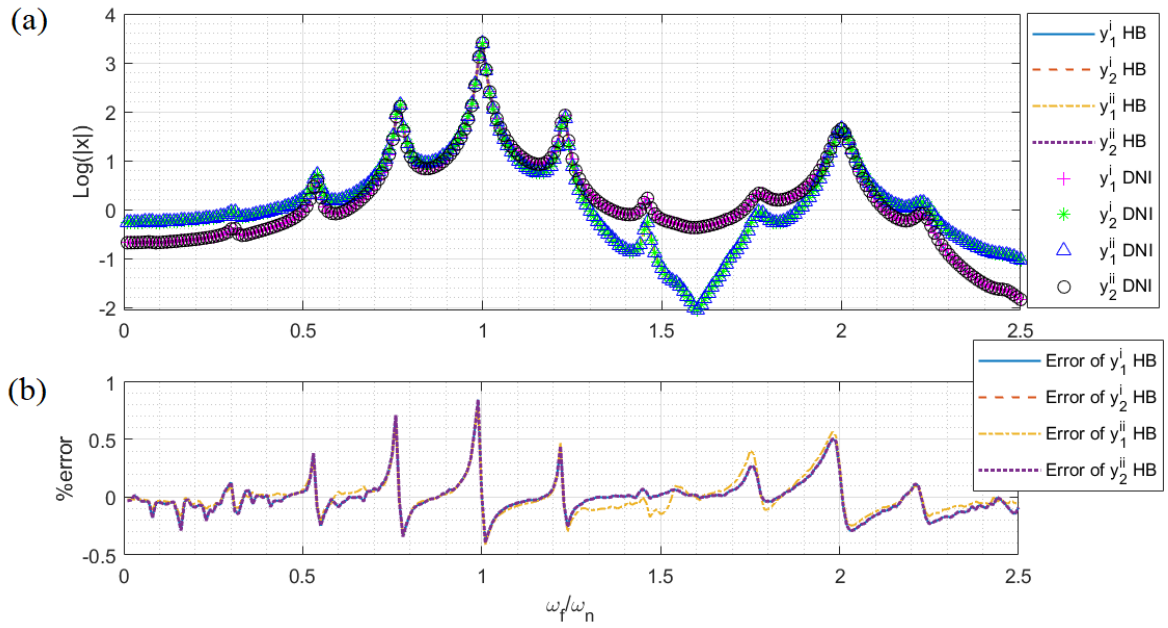

Figure 4.17: Comparing the result of reciprocity test by HB method with DNI for two degrees of freedom ($N_{HB} = 11$). (a) The logarithm of maximum amount of amplitude for all the frequency results of both methods are compared. (b) error percentages of source and receiver in compare by DNI.

The system is tested for the reciprocity as a function of the phase difference (ϕ_1, ϕ_2) between the two parametric excitation frequencies. Figure 4.18(a) shows the result of the test for five different values of ϕ_2. According to this figure, the response of the system without ϕ_2 is reciprocal, but it becomes nonreciprocal by adding the delay to the parametric excitation. In these new situations, the system's response is not reciprocal except on some particular frequencies. For example, the system behaves reciprocally far from the ANFs or on the intersections of two response curves near ANFs.

As another example, a large value of k_m is selected near the instability threshold (k_m=0.7 according to Figure 4.8). Like the first example, the response of the system with $\phi_2 = 0$ is entirely reciprocal. Increasing the ϕ_2 cause the system shows nonreciprocal behavior, except at two particular frequencies (see Figure 4.18(b)). These frequencies are not fixed and depend on the k_m, but there are near ANFs. The outcome of these two examples shows increasing the k_m can cause to increase in the nonreciprocity effect.

As Figure 4.19 shows, adding freedom degrees to this system increases the number of primary resonances and their side bonds. These primary resonances are caused by additional degrees of freedom. The reciprocity test shows the same behavior of the source and receiver with some more peaks (see Figure 4.20). The number of peaks in the reciprocity test rises by adding additional mass to the system, but the maximum nonreciprocity effect generally stays the same.

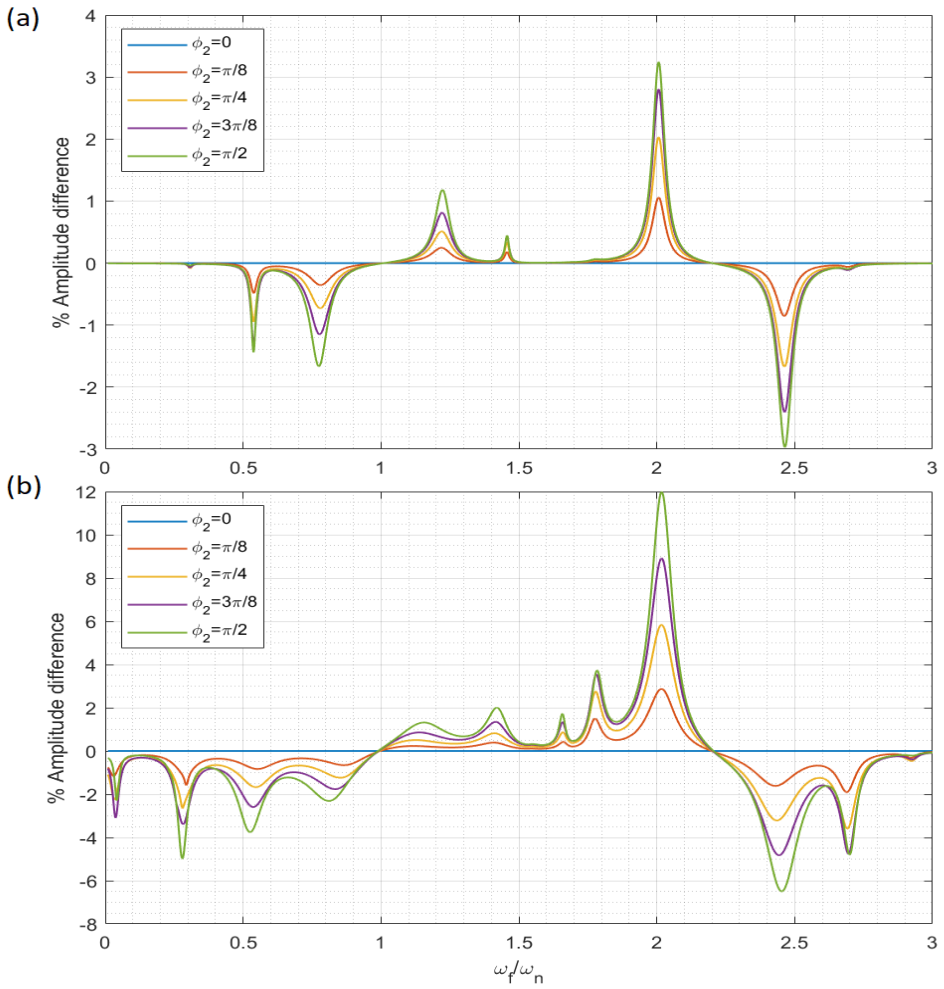

Figure 4.18: Reciprocity test in different phase angles with (a) $k_m = 0.2$, (b) $k_m = 0.7$ ($\omega_m = 0.23, k_c = 2, \zeta = 0.008$).

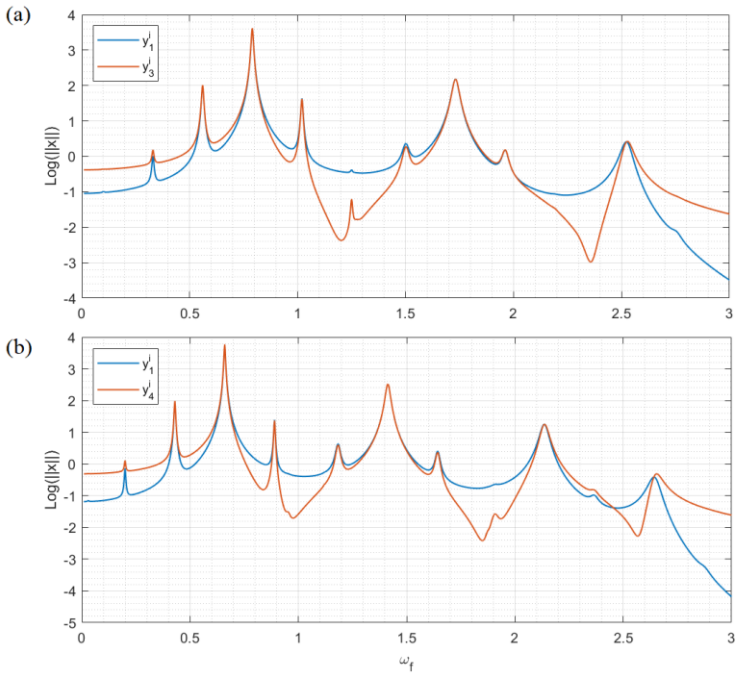

Figure 4.19: The amplitude response of source and receiver masses for (a) three degree of freedom and (b) four degrees of freedom ($\omega_m = 0.23, k_m = 0.2, k_c = 2, \zeta = 0.008$).

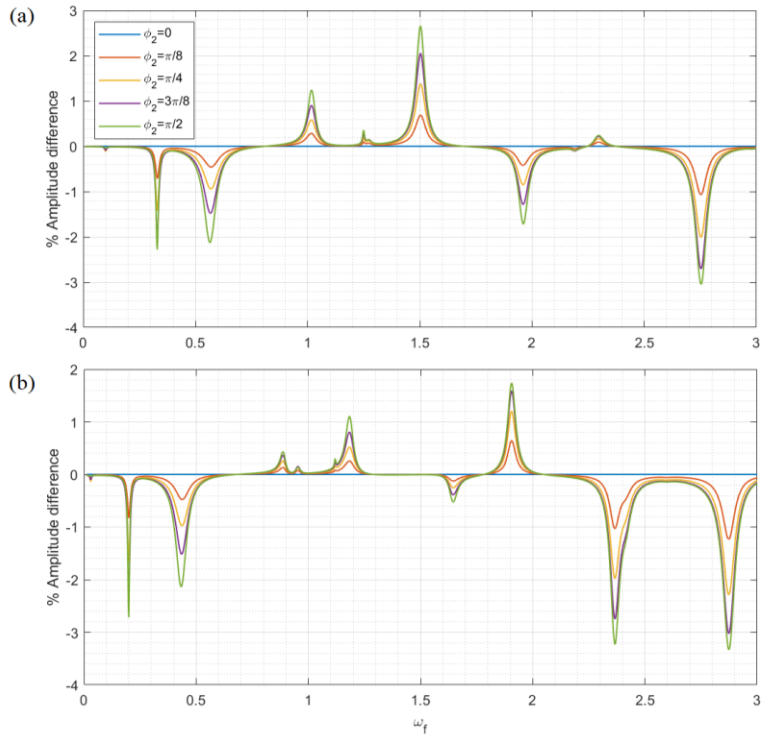

Figure 4.20: Reciprocity test in different phase angles for (a) three degrees of freedom and (b) four degrees of freedom ($\omega_m = 0.23, k_m = 0.2, k_c = 2, \zeta = 0.008$).

The response of the nonlinear system shows some unstable points, as is represented in Figure 4.21(a). The result of the non-reciprocity effect is the same as the linear oscillator with more sensitivity to the phase of modulators (see Figure 4.22).

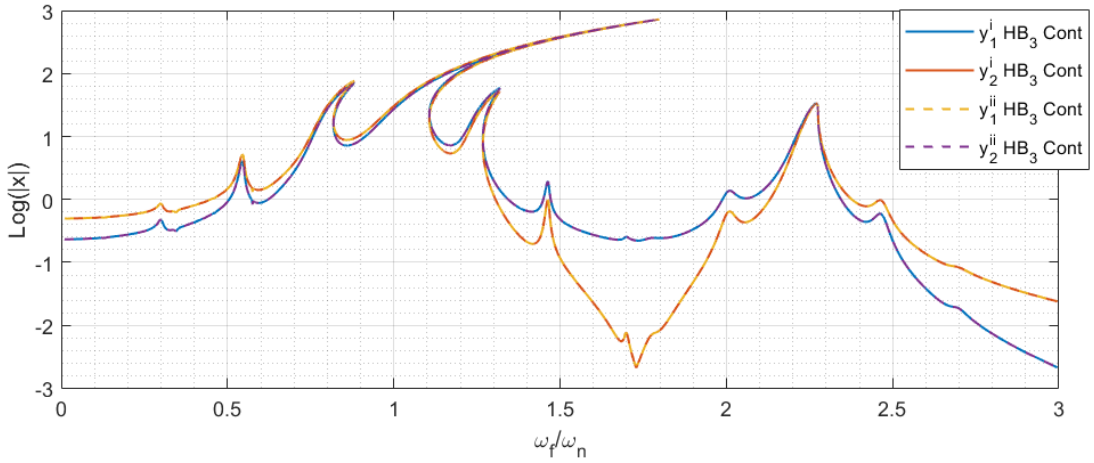

Figure 4.21: Reciprocity test in oscillator with cubic nonlinearity. The logarithmic illustrated of frequency response in both directions. ($\omega_m = 0.23,\ k_m = 0.2, k_c = 2, \zeta = 0.008, \alpha = 0.01, \phi_1 = \phi_2 = 0$).

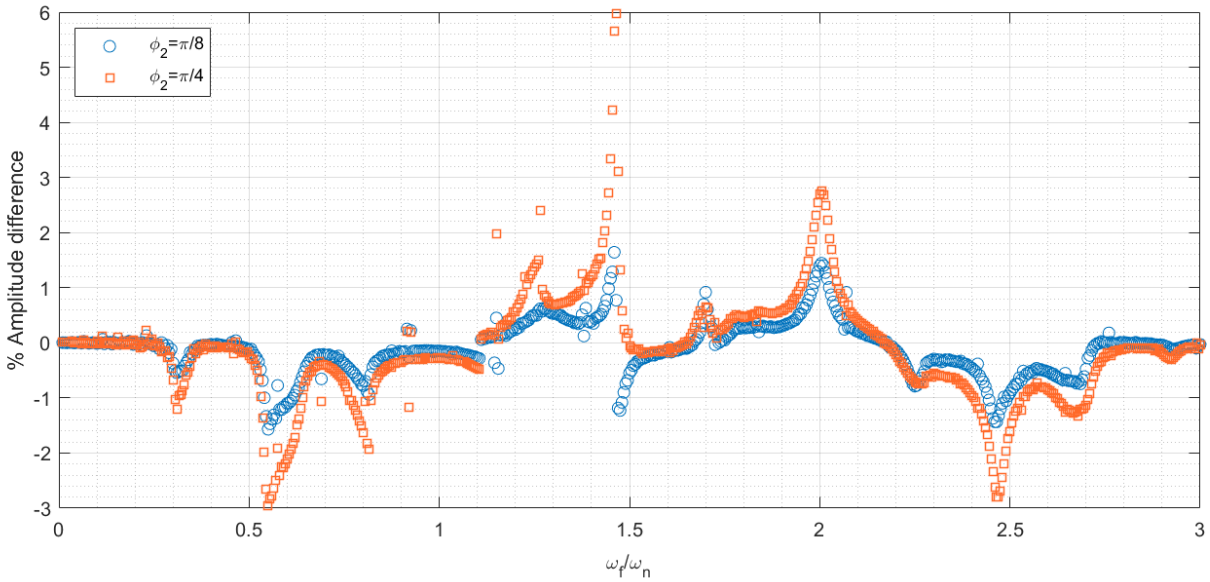

Figure 4.22: Reciprocity test in different phase angles of oscillator with cubic nonlinearity.

4.4 Summary

The main issue that separates this Chapter from others is the relationship between excitation frequencies (internal and external). This Chapter started with introducing this type of dynamic system and the difficulty of applying the HB method. The AFT technique is no longer applicable

in this Chapter because of the system's non-harmonic nature. Therefore, applying the HB needs a lot of cumbersome hand-done calculations, especially in nonlinear systems. The AHBM showed excellent agreement at linear problems in comparison with numerical results. Although using this technique in nonlinear problems did not have a good agreement with the system's dynamic, it remains helpful in showing the steady-state frequency response with acceptable accuracy.

In the last part, the validated method was used to analyze the behavior of systems with two degrees of freedom and is extended by analyzing the non-reciprocity phenomenon. This last example shows the ability of the Fourier series-based method to predict the behavior of complex phenomena.

CHAPTER 5 Conclusion

5.1 Summary of contributions

The objective of this work was to develop computer codes based on the harmonic balance (HB) method to compute the steady-state response of vibrating systems that exhibit quasi-periodic motion. The HB method is a classical approach for the analysis of the steady-state response of nonlinear structures. While the procedural aspects of the HB method are straightforward for many common types of problems involving periodic steady-state response, their application for the study of quasi-periodic dynamics is not as well established. The nature of quasi-periodic motion is different from that of periodic motion, which necessitates a different methodology for HB analysis.

In this work, the HB method was used to analyze quasi-periodic vibrations in two classes of problems: (i) a nonlinear oscillator subject to external quasi-periodic excitation, (ii) a parametrically excited system subject to external harmonic excitation. Two different scenarios were considered for the parametrically excited system: (a) when the ratio of the frequencies of parametric and external excitations is a rational number, (b) when the frequencies of parametric and external excitations can be incommensurate. While we focused on the periodic response in the first case, the response in the second case is generally quasi-periodic.

The exponential form of the multidimensional harmonic balance method (MHBM) makes the calculation of the quasi-periodic response more straightforward. In Chapter 2, we evaluated the accuracy of this method and used it to analyze the response of a system with two degrees of freedom. Moreover, the commonly used Newton-Raphson root-finding procedure was replaced with the trust-region algorithm to reduce the computation cost.

The Galerkin projection used in Chapter 3 for periodic response is not useful for HB analysis of the quasi-periodic response of forced parametric oscillator because of its non-harmonic nature. The alternating frequency time-domain (AFT) technique is inapplicable for the same reason. Nevertheless, applying the HB method by balancing the terms with the same frequency (in the style of hand calculations) still results in an acceptable approximation when a small number of harmonics are needed. This approach works well in linear problems but is very cumbersome in nonlinear problems. When effects due to higher harmonics of the modulation frequency need to be incorporated, applying the HB method is no longer feasible, and one needs to resort to perturbation methods.

In Chapter 4, we used the methodology based on two independent variables to approximate the forced parametric oscillator (FPO) with incommensurate frequencies; the adjusted harmonic balance method (AHBM). This approach can be used regardless of whether the response is periodic or quasi-periodic. After validation, the method was used for analyzing parametrically excited systems with two or more degrees of freedom. For this purpose, the reciprocity invariance was explored in linear and nonlinear systems. This short parametric study showcases the ability of the methodology developed in Chapter 4 to predict the steady-state response of complicated systems.

5.2 Suggestions for future work

While many non-periodic examples have been solved in this thesis by the HB method, there are still several unresolved issues that can be considered as current challenges or future work. We can summarize the main challenges in two categories. The first category involves advancements in the methodology of HB analysis:

(i) Performing stability analysis for the response calculated by the HB method.

(ii) Analysis of the quasi-periodic response in nonlinear problems with piecewise-smooth characteristics, such as bilinear stiffness and dry friction.

(iii) Developing efficient algorithms for the analysis of the quasi-periodic response in large systems (i.e., with many degrees of freedom).

(iv) Finding a new method to calculate the nonlinear force in forced parametric excitation problems with no relation between excitation frequencies. As the AFT method is not applicable, we need a new technique to compute the nonlinear force in the frequency domain.

Because this work was focused on developing numerical methods, certain theoretical aspects of the quasi-periodic response were not analyzed in detail. The second category of suggestions for future work is for further theoretical analysis of these aspects:

(i) We showed in Chapter 4 that the HB method cannot predict the combination resonance that occurs at a frequency between the primary and first lower sideband frequency (LSF) of the nonlinear system when the frequencies of the external and parametric forces are incommensurate. Although direct numerical simulation of the system shows

the subharmonic modulation frequency is responsible for this peak, it is not straightforward to include this term in the HB method.

(ii) In Chapter 4, we showed the effect of the super-harmonic frequency of the external excitation on the steady-state response of nonlinear force parametric systems. This effect is shown in Figure 4.9 based on direction simulation of the governing equations. It would be interesting to explore this further using the HB method.

(iii) In Section 4.3.2, only studied the effect of modulation amplitude, phase, and the external frequency on the reciprocity of the response. The numerical approach developed here can be used for further parametric studies of non-reciprocity in parametrically excited systems.

Appendix A

This appendix is about the example of applying the HB method on Duffing oscillator subject to the external harmonic force according to Chapter 1, plus a Matlab function used to solve it.

The Duffing oscillator, named after Georg Duffing [36], is a nonlinear dynamic system that is selected to explain the method. This system has a nonlinear spring in which the stiffness is a function of the displacement. As the stiffness is assumed symmetric, it is related to cubic of displacement. The equation with a periodically excited can be written in a nondimensional form as:

$$\ddot{x} + 2\zeta\dot{x} + x + \gamma x^3 = g\sin(\omega t) \tag{A.1}$$

where the ζ, γ, and g stand for damping parameter, nonlinear term coefficient, and excitation harmonic components, respectively, with the following values:

$$\zeta = 0.1, \qquad \gamma = 0.2, \qquad g = 5 \tag{A.2}$$

that the excitation harmonic component can be represented in complex form

$$g\sin(\omega t) = \frac{g}{2i}\left(e^{i\omega t} - e^{-i\omega t}\right), \tag{A.3}$$

to solve by the method that was explained. By choosing fifteen harmonic terms or only even harmonic terms until fifteen, the primary resonance and the seven super-harmonic resonances can be captured (see Fig. 0.1).

The Matlab function that is used to solve this example is based on what M. Krack and J. Gross [8] did in their book. The function is expressed as:

```
function R = Arcresidual(X,M,zeta,kappa,gamma,P,H,N,OldX,ds)
%% Conversion of sine-cosine to complex-exponential representation
Q_ce =[flipud(X(2:2:end-1)+1i*X(3:2:end-1))/2;...
              X(1);...
             (X(2:2:end-1)-1i*X(3:2:end-1))/2];

%% Excitation frequency
Om = X(end);

%% Periodic Excitation
Fex_ce = [zeros(H-1,1);1i*P/2;0;-1i*P/2; zeros(H-1 ,1)];

%% AFT for cubic spring nonlinearity
% Determine inverse discrete Fourier transform matrix
% N : number of time instants from Ref.[4] Eq.(2.19) N = 2H + 1 Ref.[4] Eq.(2.64)
E_NH = exp(1i*2*pi/N*(0:N-1)'*(-H:H));
```

```
% Apply inverse discrete Fourier transform
q = real(E_NH*Q_ce);

% Evaluate nonlinear force in the time domain
fnl = gamma*q.^3;

% Apply discrete Fourier transform
% from 2.65
Fnl_ce = E_NH'/N*fnl;

%% Dynamic force equilibrium

% The time derivative of a Fourier series is still a Fourier series of the
% same truncation order. The Fourier coefficients are just multiplied by
% kπ and rotated by pi/2.

R_ce = ( -((-H:H)'*Om).^2 * M + 1i*(-H:H)'*Om * zeta + kappa ).* Q_ce+…
    Fnl_ce-Fex_ce;

%% Arc-length calculating

Arc= ((norm(OldX - X)).^2) - (ds)^2;

%% Conversion of complex-exponential to sine-cosine representation
% R=[f(0);cosine Fourier coefficients; sine Fourier coefficients; Arc-length equation]
R = [real(R_ce(H+1));real(R_ce(H+2: end));-imag(R_ce(H+2: end));Arc];

end
```

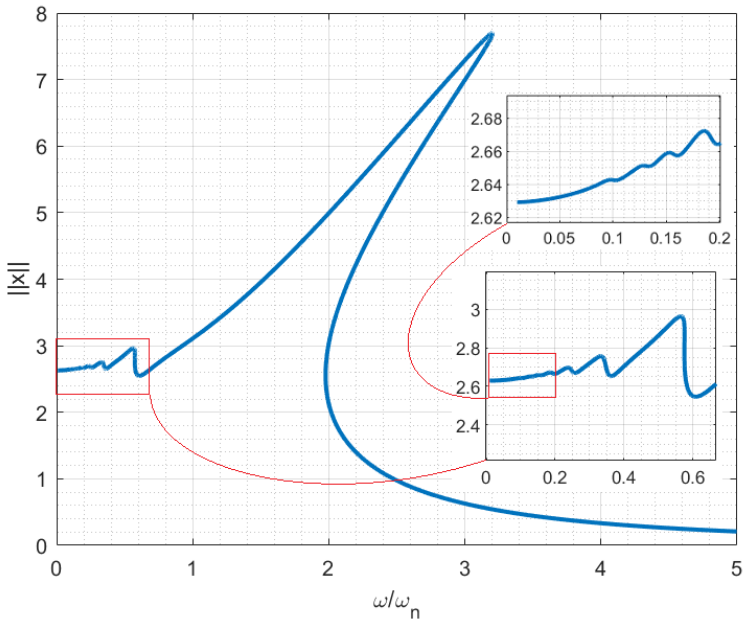

Figure 0.1: Mono-periodic-Excitation Duffing Oscillation by fifteen harmonic terms.

Appendix B

This appendix is about what we expect to see in the frequency response of the force parametric oscillators. We assume the simple answer for Eq. 4.1:

$$X = Acos(\omega_f t) \tag{B.1}$$

Substituting this assumption to the that equation yield the especial term for stiffness:

$$k_m \cos(\omega_m t) X = \frac{Ak_m}{2}\{cos((\omega_f + \omega_m)t) + cos((\omega_f - \omega_m)t)\}. \tag{B.2}$$

For capturing this term in a method like HB, terms with $(\omega_f \pm \omega_m)$ angular frequency must be added to the assumption. Additional terms also cause to terms with $(\omega_f \pm 2\omega_m)$ appear in the equation. From these calculations, we expected the frequency response of force parametric made from a series of terms with $(\omega_f \pm n\omega_m)$ angular frequency. That series can be truncated to achieve acceptable accuracy.

Appendix C

This appendix will review the Galerkin projection procedure and represents the sample MATLAB code. The general equation of motion for a nonlinear system is given as follows:

$$M\ddot{x} + C\dot{x} + Kx + f_{NL}(x, \dot{x}, t) = g(t) \tag{C.1}$$

Assume the solution of Eq. (C.1) is periodic that can be represented as a Fourier series:

$$X(t) = \sum_{k=0}^{H} \tilde{A}_x \cos(k\omega t) + \tilde{B}_x \sin(k\omega t) \tag{C.2}$$

Next, Substituting Eq. (C.2) in Eq. (C.1) yields an equation based on different harmonic of ω that need to obtain onto the sine and cosine and disregard the terms in higher frequencies than $H\omega$. To computerize this process the Galerkin projection can be useful. The scalar product of the Galerkin projection is given as follows:

$$< f, g >= \int_0^{2\pi/\omega} f(t)g(t)dt \tag{C.3}$$

A set of $n(2H+1)$ nonlinear algebraic equations can be derived by this method. A simple example of this process is presented as MATLAB code below:

```
clear;clc;close all;

syms t w A0 A1 B1 C K F real

X =A0+A1*cos(w*t)+B1*sin(w*t);

F_t = (diff(diff(X,t),t) + C*diff(X,t) + K*X + alpha*X^3) - F*cos(w*t);

F_A0 = int(F_t,t,[0 2*pi/w])

Fcos = int(F_t*cos(w*t),t,[0 2*pi/w])

Fsin = int(F_t*sin(w*t),t,[0 2*pi/w])
```

Appendix D

A solution for decoupled excitation frequencies

This section is about finding the algebraic equations from AHBM for linear system with uncoupled parametric and external forces. The explanation of method for five terms is given as follow:

$$\begin{aligned} X = A_1\cos(\omega_f t) + B_1\sin(\omega_f t) + A_2\cos((\omega_f+\omega_m)t) + B_2\sin((\omega_f+\omega_m)t) \\ + A_3\cos((\omega_f-\omega_m)t) + B_3\sin((\omega_f-\omega_m)t) \\ + A_4\cos((\omega_f+2\omega_m)t) + B_4\sin((\omega_f+2\omega_m)t) \\ + A_5\cos((\omega_f-2\omega_m)t) + B_5\sin((\omega_f-2\omega_m)t) \end{aligned} \quad (D.1)$$

Substituting the Eq. (D.1) to Eq. (4.1) by $M=1$ and without nonlinearity results to

$$
\begin{aligned}
&- A_1 w_f^2 Cos(w_f t) + B_1 Cos(w_f t) Cw_f + A_1 Cos(w_f t) k_0 + \frac{A_2 k_{mCos(w_{ft})}}{2} + \frac{A_3 k_m Cos(w_f t)}{2} \\
&- FCos(w_f t) + B_1 sin(w_f t) - A_1 sin(w_f t) Cw_f + \frac{B_2 k_m sin(w_f t)}{2} \\
&+ \frac{B_3 k_m sin(w_f t)}{2} - B_1 w_f^2 sin(w_f t) + B_2 Cos(w_f t + w_m t) Cw_f \\
&+ B_2 Cos(w_f t + w_m t) Cw_m - A_2 Cos(w_f t + w_m t) w_f^2 \\
&- A_2 Cos(w_f t + w_m t) w_m^2 + A_2 Cos(w_f t + w_m t) k_0 + \frac{A_1 k_m Cos(w_f t + w_m t)}{2} \\
&- 2A_2 Cos(w_f t + w_m t) w_f w_m + \frac{A_4 k_m Cos(w_f t + w_m t)}{2} \\
&+ B_3 Cos(w_f t - w_m t) Cw_f - B_3 Cos(w_f t - w_m t) Cw_m \\
&- A_3 Cos(w_f t - w_m t) w_f^2 - A_3 Cos(w_f t - w_m t) w_m^2 + A_3 Cos(w_f t - w_m t) k_0 \\
&+ \frac{A_1 k_m Cos(w_f t - w_m t)}{2} + 2A_3 Cos(w_f t - w_m t) w_f w_m \\
&+ \frac{A_5 k_m Cos(w_f t - w_m t)}{2} - A_2 sin(w_f t + w_m t) Cw_f - A_2 sin(w_f t + w_m t) Cw_m \\
&- B_2 sin(w_f t + w_m t) w_f^2 - B_2 sin(w_f t + w_m t) w_m^2 + B_2 sin(w_f t + w_m t) k_0 \\
&+ \frac{B_1 k_m sin(w_f t + w_m t)}{2} - 2B_2 sin(w_f t + w_m t) w_f w_m + \frac{B_4 k_m sin(w_f t + w_m t)}{2} \\
&- A_3 sin(w_f t - w_m t) Cw_f + A_3 sin(w_f t - w_m t) Cw_m - B_3 sin(w_f t - w_m t) w_f^2 \\
&- B_3 sin(w_f t - w_m t) w_m^2 + B_3 sin(w_f t - w_m t) k_0 + \frac{B_1 k_m sin(w_f t - w_m t)}{2} \\
&+ 2B_3 sin(w_f t - w_m t) w_f w_m + \frac{B_5 k_m sin(w_f t - w_m t)}{2} \\
&+ B_4 Cos(w_f t + 2w_m t) Cw_f \\
&+ 2B_4 Cos(w_f t + 2w_m t) Cw_m + \frac{A_2 k_m Cos(w_f t + 2w_m t)}{2} - 4A_4 Cos(w_f t + 2w_m t) w_f w_m \\
&+ A_4 Cos(w_f t + 2w_m t) k_0 - A_4 Cos(w_f t + 2w_m t) w_f^2 - 4A_4 Cos(w_f t + 2w_m t) w_m^2 \\
&+ B_5 Cos(w_f t - 2w_m t) Cw_f - 2B_5 Cos(w_f t - 2w_m t) Cw_m \\
&+ \frac{A_3 k_m Cos(w_f t - 2w_m t)}{2} + 4A_5 Cos(w_f t - 2w_m t) w_f w_m \\
&+ A_5 Cos(w_f t - 2w_m t) k_0 - A_5 Cos(w_f t - 2w_m t) w_f^2 - 4A_5 Cos(w_f t - 2w_m t) w_m^2 \\
&- A_4 sin(w_f t + 2w_m t) Cw_f - 2A_4 sin(w_f t + 2w_m t) Cw_m + \frac{B_2 k_m sin(w_f t + 2w_m t)}{2} \\
&- 4B_4 sin(w_f t + 2w_m t) w_f w_m + B_4 sin(w_f t + 2w_m t) k_0 - B_4 sin(w_f t + 2w_m t) w_f^2 \\
&- 4B_4 sin(w_f t + 2w_m t) w_m^2 - A_5 sin(w_f t - 2w_m t) Cw_f \\
&+ 2A_5 sin(w_f t - 2w_m t) Cw_m + \frac{B_3 k_m sin(w_f t - 2w_m t)}{2} \\
&+ 4B_5 sin(w_f t - 2w_m t) w_f w_m + B_5 sin(w_f t - 2w_m t) k_0 - B_5 sin(w_f t - 2w_m t) w_f^2 \\
&- 4B_5 sin(w_f t - 2w_m t) w_m^2 + \frac{B_5 k_m sin(w_f t - 3w_m t)}{2} + \frac{B_4 k_m sin(w_f t + 3w_m t)}{2} \\
&+ \frac{A_4 k_m Cos(w_f t + 3w_m t)}{2} + \frac{A_5 k_m Cos(w_f t - 3w_m t)}{2}
\end{aligned}
\tag{D.2}
$$

By collecting terms with the same angular frequency and disregarding terms in $Cos(w_f t \pm 3w_m t)$ and $Sin(w_f t \pm 3w_m t)$, ten algebraic equations are obtained as follow:

$$-A_1 w_f^2 + B_1 C w_f + A_1 k_0 + \frac{A_2 k_m}{2} + \frac{A_3 k_m}{2} = F \quad \text{(D.3)}$$

$$B_1 k_0 - A_1 C\, w_f + \frac{B_2 k_m}{2} + \frac{B_3 k_m}{2} - B_1 w_f^2 = 0 \quad \text{(D.4)}$$

$$B_2 C w_f + B_2 C w_m - A_2 w_f^2 - A_2 w_m^2 + A_2 k_0 + \frac{A_1 k_m}{2} - 2A_2 w_f w_m + \frac{A_4 k_m}{2} = 0 \quad \text{(D.5)}$$

$$-A_3 C w_f + A_3\, C w_m - B_3 w_f^2 - B_3 w_m^2 + B_3 k_0 + \frac{B_1 k_m}{2} + 2B_3 w_f w_m + \frac{B_5 k_m}{2} = 0 \quad \text{(D.6)}$$

$$B_3 C w_f - B_3 C w_m - A_3 w_f^2 - A_3 w_m^2 + A_3 k_0 + \frac{A_1 k_m}{2} + 2A_3 w_f w_m + \frac{A_5 k_m}{2} = 0 \quad \text{(D.7)}$$

$$-A_2 C w_f - A_2 C w_m - B_2 w_f^2 - B_2 w_m^2 + B_2 k_0 + \frac{B_1 k_m}{2} - 2B_2 w_f w_m + \frac{B_4 k_m}{2} = 0 \quad \text{(D.8)}$$

$$+B_4 C w_f + 2B_4 C w_m + A_2 \frac{k_m}{2} - 4A_4 w_f w_m + A_4 k_0 - A_4 w_f^2 - 4A_4\, w_m^2 = 0 \quad \text{(D.9)}$$

$$-A_4 C w_f - 2A_4 C w_m + \frac{B_2 k_m}{2} - 4B_4 w_f w_m + B_4 k_0 - B_4 w_f^2 - 4B_4 w_m^2 = 0 \quad \text{(D.10)}$$

$$B_5 C w_f - 2B_5 C w_m + \frac{A_3 k_m}{2} + 4A_5 w_f w_m + A_5 k_0 - A_5 w_f^2 - 4A_5 w_m^2 = 0 \quad \text{(D.11)}$$

$$-A_5 C w_f + 2A_5 C w_m + \frac{B_3 k_m}{2} + 4B_5 w_f w_m + B_5 k_0 - B_5 w_f^2 - 4B_5 w_m^2 = 0 \quad \text{(D.12)}$$

where Eq. (D.3) to (D.12) stand for $Cos(w_f t), Sin(w_f t), Cos(w_f t + w_m t), Sin(w_f t + w_m t), Cos(w_f t - w_m t), Sin(w_f t - w_m t), Cos(w_f t + 2w_m t), Sin(w_f t + 2w_m t), Cos(w_f t - 2w_m t), Sin(w_f t - 2w_m t)$, respectively.

References

[1] K. Lambeck, “The earth’s variable rotation: geophysical causes and consequences.,” *earth’s Var. Rotat. Geophys. causes consequences.*, 1980, doi: 10.1016/0031-9201(81)90054-6.

[2] A. R. Ingram and S. E. Motta, “A review of quasi-periodic oscillations from black hole X-ray binaries: Observation and theory,” *New Astronomy Reviews*, vol. 85. 2019, doi: 10.1016/j.newar.2020.101524.

[3] M. Guskov, J.-J. Sinou, F. Thouverez, and F. T. Multi, “Multi-dimensional harmonic balance applied to rotor dynamics,” *Mech. Res. Commun.*, vol. 35, pp. 537–545, 2008, doi: 10.1016/j.mechrescom.2008.05.002ï.

[4] K. Prabith and I. R. P. Krishna, “The stability analysis of a two-spool rotor system undergoing rub-impact,” *Nonlinear Dyn.*, vol. 104, no. 2, pp. 941–969, Apr. 2021, doi: 10.1007/S11071-021-06370-X/FIGURES/32.

[5] M. Urabe, “Galerkin’s procedure for nonlinear periodic systems,” *Arch. Ration. Mech. Anal.*, vol. 20, no. 2, pp. 120–152, Aug. 1965, doi: 10.1007/BF00284614.

[6] M. Urabe and A. Reiter, “Numerical computation of nonlinear forced oscillations by Galerkin’s procedure,” *J. Math. Anal. Appl.*, vol. 14, no. 1, pp. 107–140, 1966, doi: 10.1016/0022-247X(66)90066-7.

[7] S. L. Lau, Y. K. Cheung, and S. Y. Wu, “Incremental harmonic balance method with multiple time scales for aperiodic vibration of nonlinear systems,” *J. Appl. Mech. Trans. ASME*, vol. 50, no. 4, pp. 871–876, 1983, doi: 10.1115/1.3167160.

[8] M. Krack and J. Gross, *Harmonic Balance for Nonlinear Vibration Problems*. 2019.

[9] E. Sarrouy and J.-J. Sinou, “Non-Linear Periodic and Quasi-Periodic Vibrations in Mechanical Systems - On the use of the Harmonic Balance Methods,” *Adv. Vib. Anal. Res.*, no. April, 2011, doi: 10.5772/15638.

[10] L. Xie, S. Baguet, B. Prabel, and R. Dufour, “Bifurcation tracking by Harmonic Balance Method for performance tuning of nonlinear dynamical systems,” *Mech. Syst. Signal Process.*, vol. 88, pp. 445–461, May 2017, doi: 10.1016/j.ymssp.2016.09.037.

[11] T. Detroux, L. Renson, L. Masset, and G. Kerschen, “The harmonic balance method for bifurcation analysis of large-scale nonlinear mechanical systems,” *Comput. Methods Appl. Mech. Eng.*, vol. 296, pp. 18–38, Nov. 2015, doi: 10.1016/j.cma.2015.07.017.

[12] F. H. Ling, “An Alternating frequency/time domain method for calculating the steady-state response of nonlinear dynamic systems,” *Journal of Applied Mechanics, Transactions ASME*, vol. 57, no. 1. p. 251, 1990, doi: 10.1115/1.2888315.

[13] J. J. Stoker, *Nonlinear vibrations in mechanical and electrical systems*, no. v 2. Wiley, 1950.

[14] J. Moré and D. Sorensen, “COMPUTING A TRUSTREGION STEP,” *SIAM J. Sci. Comput.*, vol. 4, no. 3, pp. 553–572, 1983, Accessed: Nov. 09, 2021. [Online]. Available: https://epubs.siam.org/page/terms.

[15] S. Incerti, F. Zirilli, and F. Parisi, “A Fortran Subroutine for solving systems of nonlinear

simultaneous Equations," *Comput. J.*, vol. 24, no. 1, pp. 87–90, 1981.

[16] K. Levenberg, "A method for the solution of certain non-linear problems in least squares," *Q. Appl. Math.*, vol. 2, no. 2, pp. 164–168, 1944, doi: 10.1090/qam/10666.

[17] D. W. Marquardt, "An Algorithm for Least-Squares Estimation of Nonlinear Parameters," *J. Soc. Ind. Appl. Math.*, vol. 11, no. 2, pp. 431–441, Jun. 1963, doi: 10.1137/0111030.

[18] J. J. Moré, "The Levenberg-Marquardt algorithm: Implementation and theory," *Springer*, pp. 105–116, 1978, doi: 10.1007/bfb0067700.

[19] A. Takamatsu, R. Tanaka, H. Yamada, T. Nakagaki, T. Fujii, and I. Endo, "Spatiotemporal symmetry in rings of coupled biological oscillators of physarum plasmodial slime mold," *Phys. Rev. Lett.*, vol. 87, no. 7, pp. 78102-1-78102–4, 2001, doi: 10.1103/PhysRevLett.87.078102.

[20] S. V. Tikhov and D. V. Valovik, "Perturbation of nonlinear operators in the theory of nonlinear multifrequency electromagnetic wave propagation," *Commun. Nonlinear Sci. Numer. Simul.*, vol. 75, pp. 76–93, 2019, doi: 10.1016/j.cnsns.2019.03.020.

[21] K. Asadi, J. Yu, and H. Cho, "Nonlinear couplings and energy transfers in micro-and nano-mechanical resonators: Intermodal coupling, internal resonance and synchronization," *Philosophical Transactions of the Royal Society A: Mathematical, Physical and Engineering Sciences*, vol. 376, no. 2127. 2018, doi: 10.1098/rsta.2017.0141.

[22] K. S. Kundert, G. B. Sorkin, and A. Sangiovanni-Vincentelli, "Applying Harmonic Balance to Almost-Periodic Circuits," *IEEE Trans. Microw. Theory Tech.*, vol. 36, no. 2, pp. 366–378, 1988, doi: 10.1109/22.3525.

[23] S. Wang, P. Crouch, and D. Armbruster, "Bifurcation analysis of oscillations in electric power systems," *Proceedings of the IEEE Conference on Decision and Control*, vol. 4. pp. 3864–3869, 1996, doi: 10.1109/cdc.1996.577266.

[24] Y. B. Kim and S. K. Choi, "A multiple harmonic balance method for the internal resonant vibration of a non-linear Jeffcott rotor," *J. Sound Vib.*, vol. 208, no. 5, pp. 745–761, 1997, doi: 10.1006/jsvi.1997.1221.

[25] K. Huang, Y. Yi, Y. Xiong, Z. Cheng, and H. Chen, "Nonlinear dynamics analysis of high contact ratio gears system with multiple clearances," *J. Brazilian Soc. Mech. Sci. Eng.*, vol. 42, no. 2, p. 98, Feb. 2020, doi: 10.1007/s40430-020-2190-0.

[26] D. H. Hibner, "Dynamic response of viscous-damped multi-shaft jet engines," *J. Aircr.*, vol. 12, no. 4, pp. 305–312, 1975, doi: 10.2514/3.44448.

[27] Y. B. Kim and S. T. Noah, "Quasi-periodic response and stability analysis for a non-linear Jeffcott rotor," *J. Sound Vib.*, vol. 190, no. 2, pp. 239–253, 1996, doi: 10.1006/jsvi.1996.0059.

[28] L. Chua and A. Ushida, "Algorithms for Computing Almost Periodic Steady-State Response of Nonlinear Systems to Multiple Input Frequencies," *IEEE Trans. Circuits Syst.*, vol. 28, no. 10, pp. 953–971, 1981, doi: 10.1109/TCS.1981.1084921.

[29] R. R. Pušenjak and M. M. Oblak, "Incremental harmonic balance method with multiple time variables for dynamical systems with cubic non-linearities," *Int. J. Numer. Methods Eng.*, vol. 59, no. 2, pp. 255–292, Jan. 2004, doi: 10.1002/nme.875.

[30] M. Guskov and F. Thouverez, "Harmonic balance-based approach for quasi-periodic motions and stability analysis," *J. Vib. Acoust. Trans. ASME*, vol. 134, no. 3, 2012, doi: 10.1115/1.4005823.

[31] K. Prabith and I. R. P. Krishna, “A Time Variational Method for the Approximate Solution of Nonlinear Systems Undergoing Multiple-Frequency Excitations,” *J. Comput. Nonlinear Dyn.*, vol. 15, no. 3, 2020, doi: 10.1115/1.4045944.

[32] T. Rook, “An alternate method to the alternating time-frequency method,” *Nonlinear Dyn.*, vol. 27, no. 4, pp. 327–339, 2002, doi: 10.1023/A:1015238500024.

[33] H. Liao, Q. Zhao, and D. Fang, “The continuation and stability analysis methods for quasi-periodic solutions of nonlinear systems,” *Nonlinear Dyn.*, vol. 100, no. 2, pp. 1469–1496, 2020, doi: 10.1007/s11071-020-05497-7.

[34] M. Legrand and M. L. Mod, “Mod ` eles de pr ´ ediction de l ’ interaction rotor / stator dans un moteur d ’ avion To cite this version : Thèse de Doctorat,” 2006.

[35] G. Duffing, “Erzwungene schwingungen bei veränderlicher eigenfrequenz und ihre technische bedeutung,” *Braunschweig Vieweg*, vol. 41, p. 42, 1918.

[36] T. D. Equation and N. Oscillators, *Ivana Kovacic, Michael J. Brennan-The Duffing Equation_ Nonlinear Oscillators and Their Behaviour-John Wiley and Sons (2011)*. 2011.

[37] W. B. Case, “The pumping of a swing from the standing position,” *Am. J. Phys.*, vol. 64, no. 3, pp. 215–220, 1996, doi: 10.1119/1.18209.

[38] Y. A. Amer, H. S. Bauomy, and M. Sayed, “Vibration suppression in a twin-tail system to parametric and external excitations,” *Comput. Math. with Appl.*, vol. 58, no. 10, pp. 1947–1964, 2009, doi: 10.1016/j.camwa.2009.07.090.

[39] V. Ramakrishnan and B. F. Feeny, “Resonances of a forced Mathieu equation with reference to wind turbine blades,” *J. Vib. Acoust. Trans. ASME*, vol. 134, no. 6, pp. 1–14, 2012, doi: 10.1115/1.4006183.

[40] J. F. Rhoads and S. W. Shaw, “The impact of nonlinearity on degenerate parametric amplifiers,” *Appl. Phys. Lett.*, vol. 96, no. 23, pp. 6–9, 2010, doi: 10.1063/1.3446851.

[41] V. Ramakrishnan and B. F. Feeny, “Second order perturbation analysis of a forced nonlinear Mathieu equation,” *Proc. ASME Des. Eng. Tech. Conf.*, vol. 1, no. PARTS A AND B, pp. 1073–1082, 2012, doi: 10.1115/DETC2012-71532.

[42] S. Neumeyer, V. S. Sorokin, and J. J. Thomsen, “Effects of quadratic and cubic nonlinearities on a perfectly tuned parametric amplifier,” *J. Sound Vib.*, vol. 386, pp. 327–335, 2017, doi: 10.1016/j.jsv.2016.09.013.

[43] G. G. Tehrani, C. Gastaldi, and T. M. Berruti, “Trained Harmonic Balance Method for Parametrically Excited Jeffcott Rotor Analysis,” *J. Comput. Nonlinear Dyn.*, vol. 16, no. 1, 2021, doi: 10.1115/1.4048578.

[44] K. Yi, S. Karkar, and M. Collet, “One-way energy insulation using time-space modulated structures,” *J. Sound Vib.*, vol. 429, pp. 162–175, 2018, doi: 10.1016/j.jsv.2018.05.017.

[45] I. Kovacic, R. Rand, and S. M. Sah, “Mathieu’s equation and its generalizations: Overview of stability charts and their features,” *Appl. Mech. Rev.*, vol. 70, no. 2, 2018, doi: 10.1115/1.4039144.

[46] H. Lamb, “On reciprocal theorems in dynamics,” *Proc. London Math. Soc.*, vol. s1-19, no. 1, pp. 144–151, Nov. 1887, doi: 10.1112/plms/s1-19.1.144.

[47] J. D. Achenbach, *Reciprocity in Elastodynamics*. 2004.

[48] H. Nassar *et al.*, "Nonreciprocity in acoustic and elastic materials," *Nature Reviews Materials*, vol. 5, no. 9. pp. 667–685, 2020, doi: 10.1038/s41578-020-0206-0.

[49] Y. Wang, B. Yousefzadeh, H. Chen, H. Nassar, G. Huang, and C. Daraio, "Observation of Nonreciprocal Wave Propagation in a Dynamic Phononic Lattice," *Phys. Rev. Lett.*, vol. 121, no. 19, 2018, doi: 10.1103/PhysRevLett.121.194301.